MONITORING FOLDING PATHWAYS FOR LARGE RNAS USING SITE-DIRECTED SPIN-LABELING TECHNIQUES

A Thesis

by

CARRÉ ALISON ZALMA

Submitted to the Office of Graduate Studies of
Texas A&M University
in partial fulfillment of the requirements for the degree of

MASTER OF SCIENCE

December 2005

Major Subject: Chemistry

MONITORING FOLDING PATHWAYS FOR LARGE RNAS USING SITE-DIRECTED SPIN-LABELING TECHNIQUES

A Thesis

by

CARRÉ ALISON ZALMA

Submitted to the Office of Graduate Studies of
Texas A&M University
in partial fulfillment of the requirements for the degree of

MASTER OF SCIENCE

Approved by:

Chair of Committee	Victoria J. DeRose
Committee Members,	David H. Russell
	Eric E. Simanek
	David P. Giedroc
Head of Department,	Emile A. Schweikert

December 2005

Major Subject: Chemistry

ABSTRACT

Monitoring Folding Pathways for Large RNAs Using Site-Directed Spin-Labeling Techniques. (December 2005)

Carré Alison Zalma, B.S., Eastern Michigan University

Chair of Advisory Committee: Dr. Victoria J. DeRose

The function of biomolecules is very sensitive to structure. Folding in proteins and nucleic acids is a hierarchical process progressing from primary to secondary, then tertiary, and finally, quaternary structures. RNA in its folded form performs a variety of biological activities. Obtaining intramolecular distance measurements makes it possible to generate structural models along the folding pathway that may be related to the overall function of the molecule. Distances can be measured by Site-Directed Spin-Labeling (SDSL), in which nitroxyl spin-label probes are attached and observed by EPR spectroscopy. Spin-labels can provide information concerning structure and conformational changes because they are particularly sensitive to molecular motion and interspin distances. Continuous-wave EPR spectroscopy has been commonly applied to detect and monitor nitroxide spin-label probes within biological systems.

A previous published SDSL study from this laboratory investigated a 10-mer RNA duplex model system with spin-label probe succinimdyl-2,2,5,5-tetramethyl-3-pyrroline-1-oxyl-carboxylate; however, an increased spin-labeling efficiency was observed with an isocyanate derivative of tetramethylpiperidyl-N-oxy (TEMPO). In this thesis, a 4-isocyano TEMPO spin-label probe replaced the previously used succinimdyl-2,2,5,5-tetramethyl-3-pyrroline-1-oxyl-carboxylate in 10-mer SDSL studies. The influence of labeling with the 4-iscocyano TEMPO spin-label in a 10-mer RNA model system was investigated with thermal denaturation, Matrix Assisted Laser Desorption Time of Flight Mass Spectrometry (MALDI-TOF-MS), Electron Paramagnetic Resonance (EPR) spectroscopy, and reverse phase high performance liquid chromatography (RP-HPLC).

In the 10-mer RNA duplex model system a 4-isocyano TEMPO spin-label is individually attached to one strand and two strands are annealed to measure distances. This methodology is limited to systems in which two oligonucleotides are annealed together. To circumvent this limitation and also to explore single-strand dynamics a new methodology was implemented, double spin-labeling. Double spin-labeled single-stranded RNA was investigated as a single-strand and within a duplex *via* MALDI-TOF-MS, EPR spectroscopy and RP-HPLC. A double spin-labeling strategy in this work will be applicable to large complex RNAs like Group I intron of *Tetrahymena thermophilia*.

DEDICATION

This thesis is dedicated to a great number of individuals who have been instrumental in my quests whether they are scholarly, athletic or social. I would particularly like to honor the recent passing of two men who were brilliant in their own right, William E. VanBlaircum and Louis V. Zalma, my grandpas.

ACKNOWLEDGEMENTS

I would like to thank my advisor, Dr. Victoria J. DeRose, for taking me under her wing when I thought that success in graduate school was lost. I would also like to thank my thesis committee, Dr. David H. Russell, Dr. Eric Simanek, and Dr. David P. Giedroc. I would also like to acknowledge Dr. Richard Crooks for sitting in on my seminar and preliminary committees in addition to all the candid conversations that we had about life and study.

I would also like to thank past and present DeRose group members. First, I would like to say what an exciting time it has been to be a part of the "Final Four" and I hope that each continues their success. Nak-Kyoon, I really appreciate all of the time and effort you spend in answering my questions and showing me things that are an old hat for you, in addition to our late night lab time where you made me laugh constantly despite the hour. Janell, I am so lucky to have had a lab Mom like you and I am grateful for all of things that you have done for me. Cynthia, I always treasure our private talks and inside jokes- I wish you all the best. Shannie, thank you for all the time you spent developing a genuine personal relationship with me, you are such a great role model and I am really glad that we were labmates. Sara, I will always remember our graduate days fondly and wish that we could always be first years together. Kendra, I am so happy that we are buddies and don't worry, you are going to do great things. Ryan, thanks for always making me look on the bright side of things. De-Roc, I cannot begin to thank you for all the wonderful things that you have done in the past year, but most of all, I really appreciate all the questions that you ask me. Lea, I really appreciate our friendship that exists in-and-out of the work environment.

I am eternally grateful to have made such wonderful friends in graduate school. Nellie, you are my best friend and I don't know what I would do without you. Nathan, I am so glad to have someone to work on projects with me regardless of what time we start them. You have been really supportive during this very stressful time and I really appreciate it. Francisco, I will always come to you for fashion and etiquette advice. T.K., I really appreciate the opportunities we have had to drive across the country together during the holiday season, it is a true test of friendship to be in a car for 18 hours.

J.Ogle thanks so much for your candor and sarcasm about any matter. Craig and Joanna, all I can say is SBSW. Patrick and Thomas, I will never forget our notorious potlucks and late-night discussions about politics and religion. I would also acknowledge Sandra Horton for her volume of experience and patience in personal and professional matters.

I would also like to thank my family for their never-ending question, “When are you going to be done with school?” Mom, thanks for always thinking that I can be anything that I want to be. Dad, thanks for always showing me how to do things that most females never tackle. Melissa and Hayley, thank you for making my trips back to Michigan exciting. Ali-Bean, I am so lucky to have such a wonderful niece who can erase all the stress of graduate school with a simple smile.

Richard, your critiques of all the drafts I passed across your desk and insight into Organic chemistry I can never repay. In this writing process I have really appreciated all the times that you listened to me when I was stressed, and all the wonderful meals that you prepared when I had forgotten about food. I know that things are never easy for either of us because we have those looming black clouds that follow, but I am glad that we are under them together.

TABLE OF CONTENTS

CHAPTER Page

LIST OF FIGURES

FIGURE Page

FIGURE Page

LIST OF TABLES

CHAPTER I
INTRODUCTION

Ribonucleic acid

The function of biomolecules is very sensitive to structure. Folding in proteins and nucleic acids is a hierarchical process progressing from primary to secondary, then tertiary and finally quaternary structures (Misra and Draper 1998). The development of structural stability in biological systems is based on a variety of factors. Specifically, electrostatic interactions play a significant role in the formation of higher order ribonucleic acid (RNA) structure. RNA in its folded form performs a variety of biological activities in gene regulation, including governing replication in viruses such as the hepatitis delta virus (HDV) and human immunodeficiency virus (HIV) (Fedor and Williamson 2005). Examples of catalysis by RNA are found in the spliceosome, in self-splicing of the Group I intron, and in peptide bond synthesis within the ribosome.

Ribonucleic acid is composed of nucleotides containing a ribose sugar, a phosphate group, and one of four bases. RNA contains four nucleobases: two pyrimidine bases, cytosine (C) and uracil (U), and two purine bases, adenine (A) and guanine (G) (Figure 1-1). RNA is synthesized in the absence of a complementary strand and this single-stranded RNA can fold back upon itself and adopt a variety of unique folds. Therefore understanding how a linear strand of RNA folds into secondary and tertiary structures is of interest. Some forces that stabilize RNA structures include base-pairing, base stacking, and ionic interactions. Traditional Watson-Crick base-pairing interactions known in DNA also occur in RNA where G hydrogen-bonds to C and A pairs with U. The phosphate backbone is a key structural component that contributes to prevalent electrostatic forces that influence RNA folding. The electrostatic repulsion between the negatively charged phosphate moieties can be minimized by the addition of counter ions such as mono- or divalent metal ions which are often required for RNA folding.

This thesis follows the style of *RNA*.

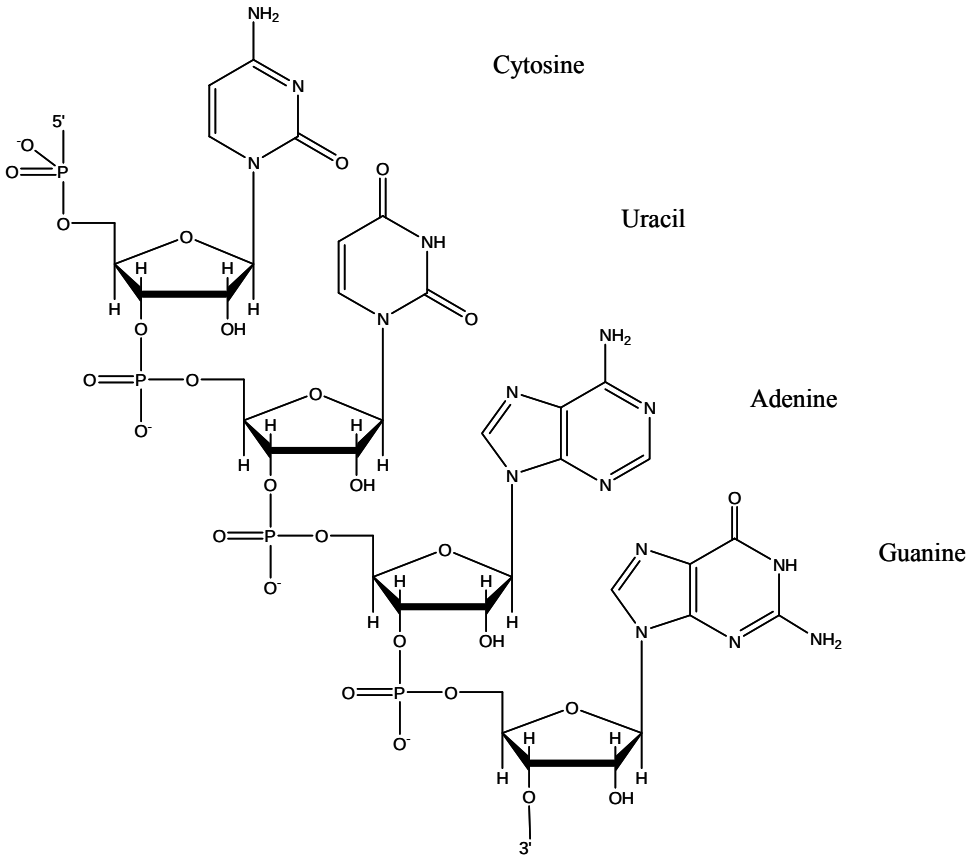

Figure 1-1: Structure of RNA. RNA contains four nucleobases: two pyrimidine bases, cytosine and uracil, and two purine bases, adenine and guanine.

The three modes of metal binding to RNA are diffuse, outer-sphere complexation and inner-sphere complexation (Misra and Draper 1998, Tinoco and Bustamante 1999, Pyle 2002, Draper 2004). Diffuse ion binding describes a mobile layer of cations that act as a screen, through water molecules, to reduce the repulsion between neighboring negatively charged phosphates. Outer-sphere complexation is similar to diffuse binding; however the ion and ligand share the same solvation sphere. An inner-sphere complex pertains to a direct contact between the ion and ligand without solvent intervening. These different modes of binding are not isolated, and therefore all act to influence RNA structure and folding.

Many folded RNA systems have been shown to act as biological catalysts (DeRose 2002, DeRose 2003, Lilley 2003). Catalytic RNAs (ribozymes) are placed into different subgroups based on size and reactivity. The "small" ribozymes (~ 40-150

nucleotides), such as the hairpin (HP), hammerhead (HH), and hepatitis delta virus (HDV), perform site-specific phosphodiester bond cleavage reactions (Figure 1-2A). The "large" ribozymes (200-500 nucleotides), including the Group I and Group II introns, mediate RNA splicing by a series of sequential phosphodiester bond cleavage reactions followed by a ligation reaction (Figure 1-2B) (Tanner 1999). Despite the limitation of chemical groups in RNA in comparison to proteins, the structural complexity of RNA aids in its ability to catalyze a multitude of chemical reactions (Kruger et al. 1982, Lohse and Szostak 1996, Wiegand et al. 1997, Unrau and Bartel 1998, Doudna and Cech 2002, Draper 2004).

The techniques described in this thesis will eventually be applied to studying folding in large RNA systems. One such system that provides an interesting metal dependent folding pathway that can be investigated with these techniques is the Group I intron ribozyme. The genes of eukaryotes contain coding sequences known as exons, which are interrupted by intervening sequences (IVS) or introns. Introns are untranslated sequences that must be removed before translation, in the process known as RNA splicing (Figure 1-3). In eukaryotes, RNA-protein complexes within the spliceosome remove the IVS. In 1982, Cech and Altman discovered that RNA could be catalytic, forming molecules called ribozymes (Kruger et al. 1982, Guerrier-Takada et al. 1983.) Specifically Cech and coworkers found that the Group I intron of *Tetrahymena thermophilia* was a self-splicing catalytic RNA that did not require proteins for splicing (Kruger et al. 1982). The Group I introns mediate the splicing of the pre-mRNA by two transesterification reactions that result in the excision of the intron and the ligation of the flanking exon sequences (Kruger et al. 1982, Cech 1990).

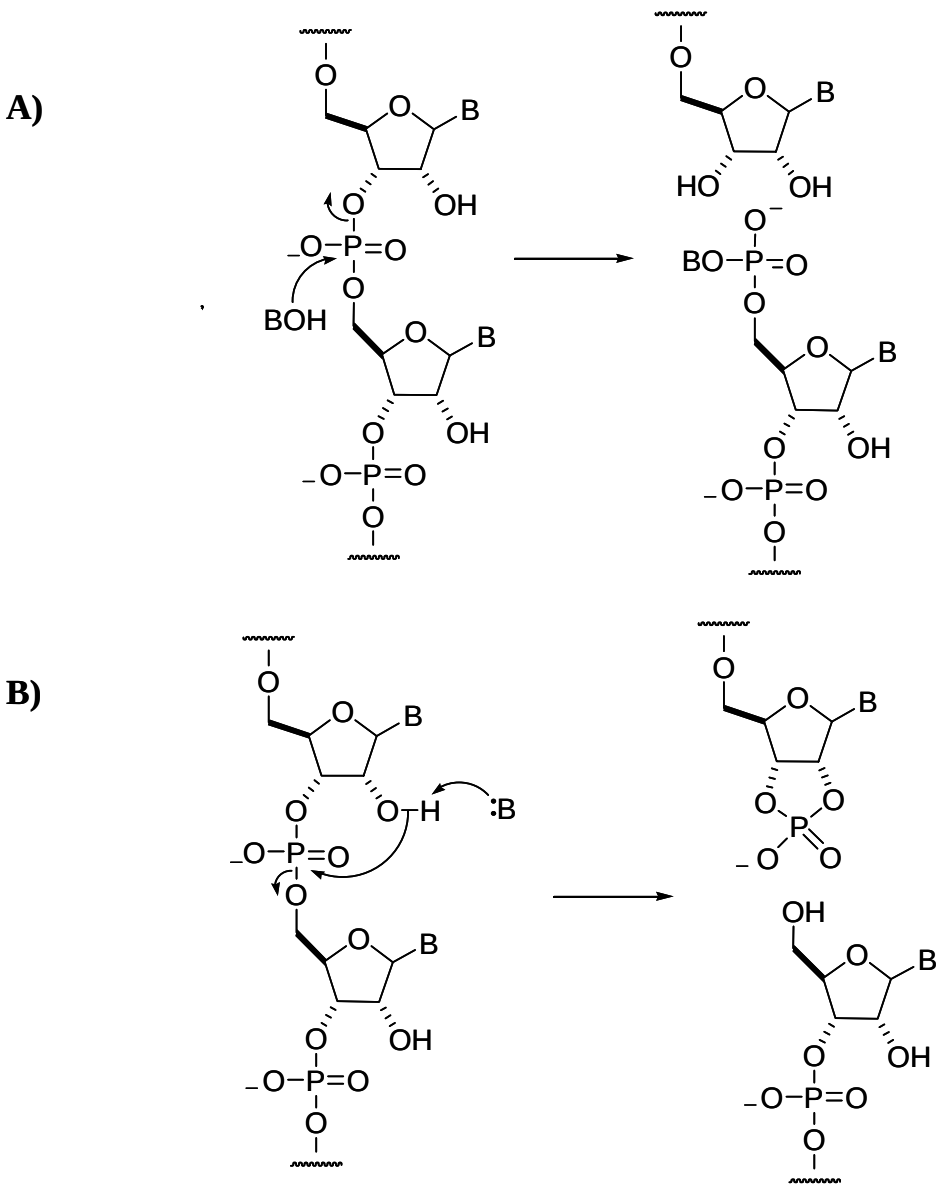

Figure 1-2: Concerted reaction mechanism for reactions catalyzed by ribozymes. The nucleophile is depicted as (:B). A) The reaction mechanism of the large ribozymes. B) The reaction mechanism of the small ribozymes.

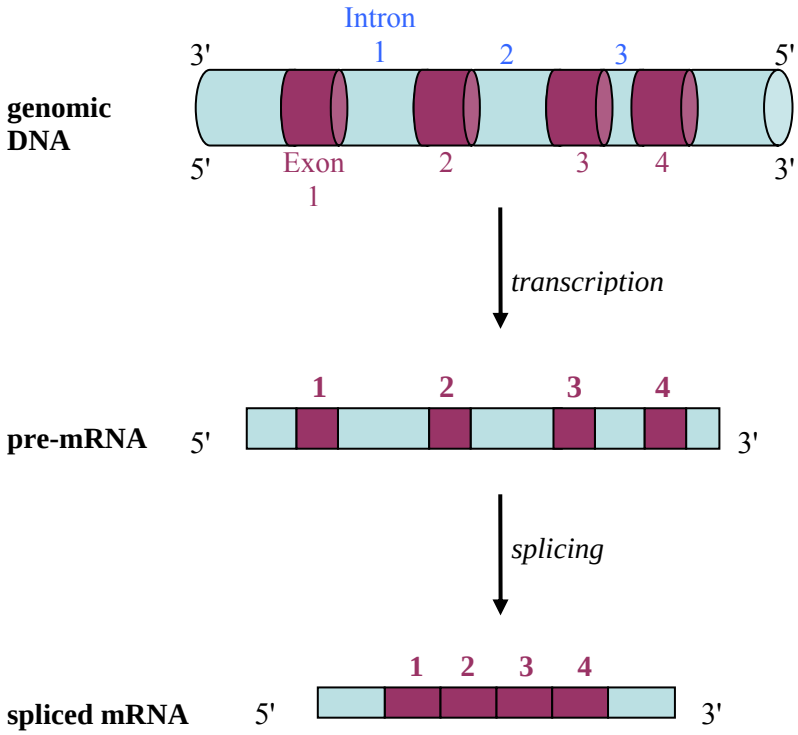

Figure 1-3: Typical splicing diagram (adapted from Watson et al. 2004). Genomic DNA is contains introns and exons. Transcription of DNA forms pre-mRNA, which is then spliced to form mRNA.

The catalytic core of Group I introns are comprised of two main structural domains, base paired (P) regions P3-P9 and P4-P6 (Doudna and Cech 1995). The secondary structure of the Group I intron of the *Tetrahymena thermophilia* is shown in Figure 1-4 (Schroeder et al. 2004). The P4-P6 domain of the Group I intron from *Tetrahymena thermophilia* is of interest due to its well-characterized folding (Burns 2004). The P4-P6 domain contains helical segments P4, P5, and P6 and also a P5abc subdomain. A 2.8 Å resolution crystal structure of the P4-P6 domain from the *Tetrahymena thermophilia* group I intron was solved by Doudna and co-workers in 1996 (Figure 1-5) (Cate et al. 1996, Cate et al. 1997). An interesting feature of the crystal structure is the predicted clustering of six magnesium ions in the P5abc subdomain. Isolated P4-P6 does not perform the self-splicing/cleavage reactions, but it is suggested

that subdomain folding is required to stabilize the active conformation needed for catalytic activity of the group I intron (Cate et al. 1996, Cate et al. 1997).

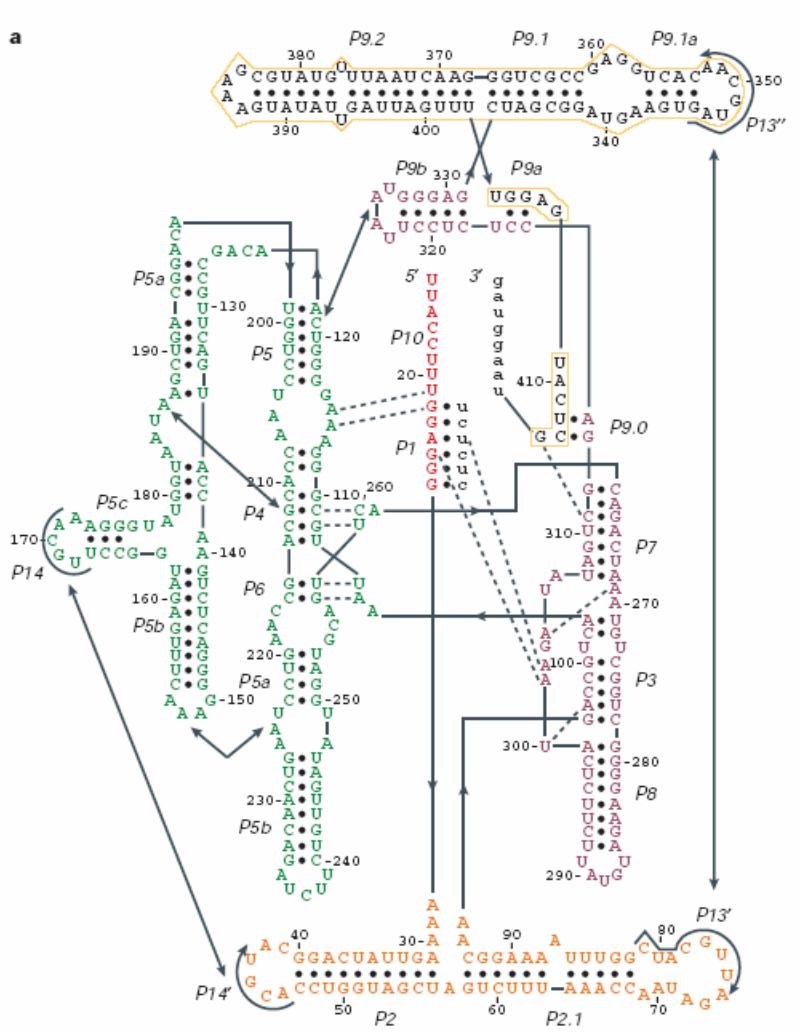

Figure 1-4: Secondary structure of the Group I intron from *Tetrahymena thermophilia* (Schroeder et al. 2004). Dashed lines indicate tertiary interactions within the catalytic core. The P4-P6 domain is in the green text and the P3-P9 domain is in purple text.

The P4-P6 domain and the P5abc subdomain have served as models for RNA folding and metal interactions. Structural characteristics of the P5abc subdomain include an A-rich bulge, a GAAA tetraloop, and a junction of helices P5a, P5b and P5c. The subdomain three helix junction protects the A-rich bulge which, according to the x-ray

crystal structure, makes a corkscrew turn to form key tertiary interactions between the helical halves of the P4-P6 domain (Doherty and Doudna 2000). Further, solution NMR spectra monitoring of the P5abc subdomain reveal a secondary structure rearrangement upon addition of divalent metal ions to form the tertiary structure (Wu and Tinoco 1998). It is suggested that the presence of the magnesium ions organize the 3-helix junction and drive the folding pathway (Wu and Tinoco 1998, Doherty and Doudna 2000). Therefore the group I intron may fold around a metal ion core rather than a hydrophobic core. A previous spectroscopic investigation of the metal ion core will set precedence for predicting the metal-dependent folding pathway (Burns 2004).

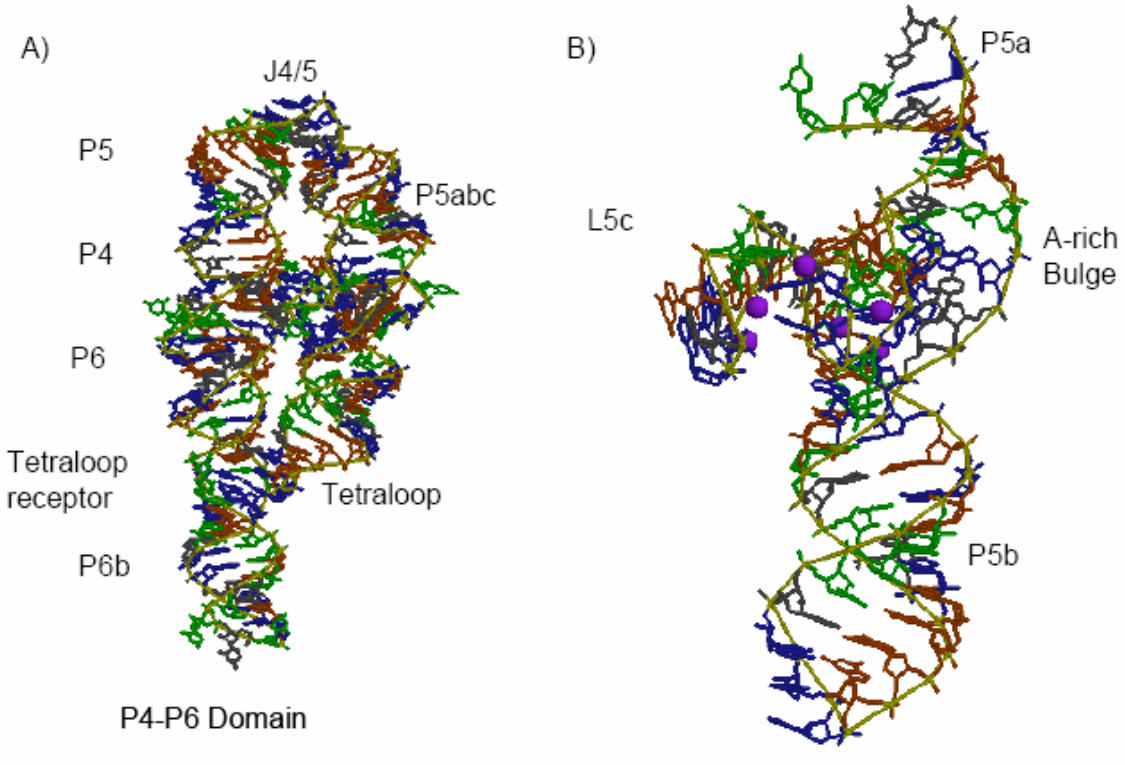

Figure 1-5: The P4-P6 domain and the P5abc subdomain. A) 2.8 Å crystal structure of the P4-P6 domain (PDB 1G1D). B) P5abc subdomain excised from the P4-P domain. Six magnesium ions are denoted as purple spheres.

Methods for studying folding processes

Insights into the mechanisms of biopolymers can be obtained from structural studies. Spectroscopic methods, such as Fluorescence Resonance Energy Transfer (FRET) and Electron Paramagnetic Resonance (EPR), implement fluorophores and spin-label probes respectively, to investigate structural changes. The FRET methodology requires attachment of two different fluorophores termed a donor-acceptor pair. In this method, fluorophores are attached to specific sites and distances are obtained based on the efficiency of energy transfer between the donor-acceptor pair (Hubbell et al. 1998, Bassi et al. 1999, Walter 2001, Wilson and Lilley 2002, Miller 2005). An advantage of this method is the ability to measure distances up to ~80 Å which made it attractive to investigate the folding pathways of the HP, HH, and HDV ribozymes (Bassi et al. 1999, Wilson et al. 2002). However, fluorophores are comparable in size to a single nucleotide and this bulkiness has potential for perturbing the RNA structure.

Site-Directed Spin-Labeling (SDSL) is an alternative distance measurement method that uses spin-label probes. SDSL is useful for mapping elements of structure that are not accessible by classical methods such as NMR and X-ray crystallography (Qin and Dieckmann 2004, Dugas 1977, Stone et al. 1965). In this method, a spin-probe with a stable paramagnetic group is attached to designated position(s) of the biomolecule and the motion of the probe is monitored with EPR spectroscopy. Through SDSL, information about the mobility of the spin-probe and distances between probes can be obtained. Some of the earliest spin-labeling with nitroxide probes dates to 1965 (Stone et al. 1965). Preliminary publications reported studying the molecular motion of the nitroxide radical on poly-L-lysine at various pH's (Stone *et al.* 1965). Initial spin-labeling studies of nucleic acids were performed in 1967 with a polyguanine system (Smith and Yamane 1967). The 1967 work implemented five and six member sized rings and additional side chain variables in a nitroxide probe system (Smith and Yamane 1967). However, spin-labeling was heavily dependent on the reactivity of the bases at various pH's and the spin-labeling efficiency was a meager 5%.

Later in 1969, a seminal RNA SDSL study was performed within transfer RNA (tRNA) (Hoffman et al. 1969). tRNA plays a central role with the ribosome in the translation of genetic information into proteins, and therefore understanding structural

rearrangements necessary for function is of interest. A succinimidyl-2,2,5,5-tetramethyl-3-pyrroline-1-oxyl-carboxylate spin-label **(1)** was synthesized and combined with the α-amino group of valyl-tRNA through an amide linkage. The dynamic motion of the spin-label with tRNA was investigated under varying ionic and temperature conditions. From this study it was possible to monitor the structural rearrangement in part of the tRNA molecule while the remainder is relatively unperturbed.

Currently, a variety of spin-label probes are used to monitor structure and dynamics using SDSL methodologies (Hubbell et al. 1998, Hustedt and Beth 1999). Proteins have been a large focus of spin-labeling and amino acids have a higher number of functionalities for specific spin-probe attachment (Altenbach et al. 1990). Proteins are generally more extensively studied biopolymers compared to RNA and as a result much success has been attributed to spin-labeling proteins with a reactive thiol group at cysteine residues (Hubbell et al. 2000). Conversely, RNA is limited to four bases which tend to be stacked and/or hydrogen bonded and this can promote difficulty in spin-labeling. For oligonucleotides, spin-labels can be incorporated to 3' and 5' termini, in addition to selective internal backbone, sugar and base positions as shown in Figure 1-6 (Macosko et al. 1999, Edwards et al. 2001a, Qin et al. 2003).

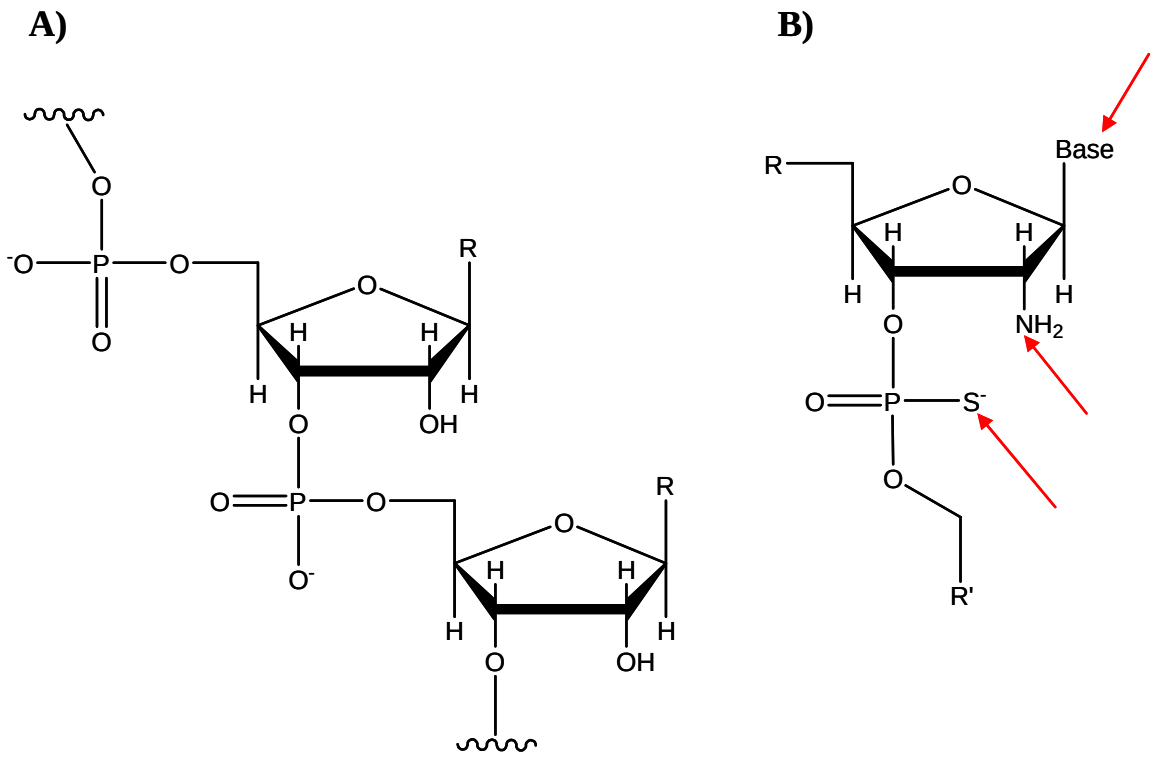

Figure 1-6: Sites for spin-label incorporation within RNA. A) Native RNA sequence with a ribose sugar, phosphate backbone and nucleobase (R). B) Red arrows denote positions for spin-label attachment to a modified RNA nucleotide.

Spin-labeling studies are helpful to gain insights in the dynamics and distance measurements within a biomolecule. Dynamic information is obtained by observing the EPR line shape of the nitroxide probe. In particular, monitoring the shape of EPR-SDSL spectra can provide information about binding and the local environment. In the absence of an applied magnetic field the m_S values are degenerate (Figure 1-7). When the magnetic field is applied Zeeman splitting occurs and ($\Delta m_S = \pm 1$) transitions are allowed between the m_S states upon application of appropriate microwave frequencies. The interaction between the nuclear and electron spin is reflected in hyperfine structure. In the case of a nitroxide radical, ^{14}N (I = 1), the EPR spectrum is split in three lines of equal intensity because the ^{14}N nucleus has three possible spin states (-1, 0, 1).

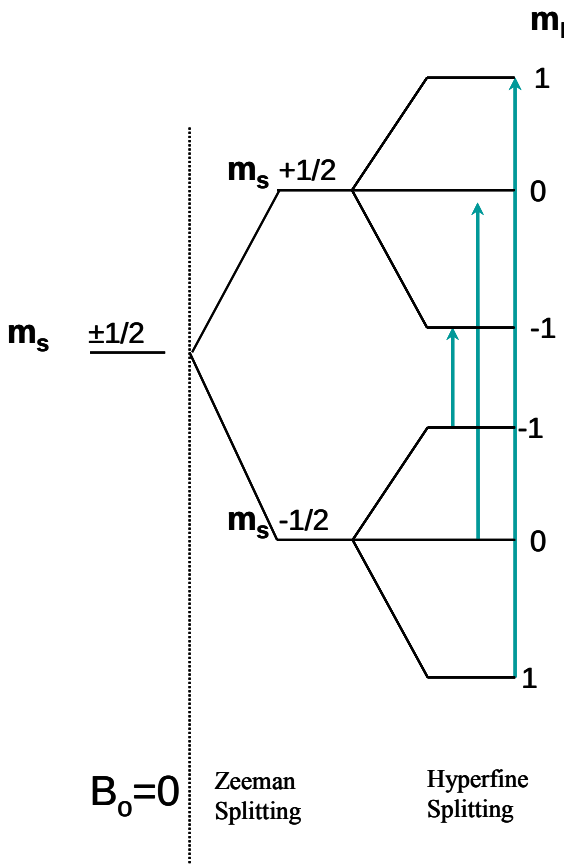

Figure 1-7: Energy level splitting diagram for nitroxide radicals.

A diagram of the EPR experimental design and representative spectra are shown in Figure 1-8. The hyperfine splitting (a) is the distance between peaks. The g-value is reflective of the electron environment and determines the center of the spectrum. Nitroxide probes have axially symmetric electron environments and two very similar g-values, g_z and $g_{x,y}$. In comparison, the hyperfine values A_z and $A_{x,y}$ are more distinguishable. The anisotropy in these values makes the nitroxide EPR spectrum sensitive to the motion of the probe during the measurement. For example, an unrestricted nitroxide spin-label in solution possesses a fast ($\tau_c \sim 10^{10}$-10^8 sec^{-1}) and uninhibited motion that generates three sharp and narrow lines due to an averaging of orientations on the X-band EPR scale. In contrast, a restricted spin-probe has a slower rotation ($\tau_c < 10^8$ sec^{-1}) and the EPR detects the distribution of the orientations, which

produces wider and shallow peaks from line broadening. Further, dipole-dipole interactions between two spin-labels in an RNA duplex can cause line broadening.

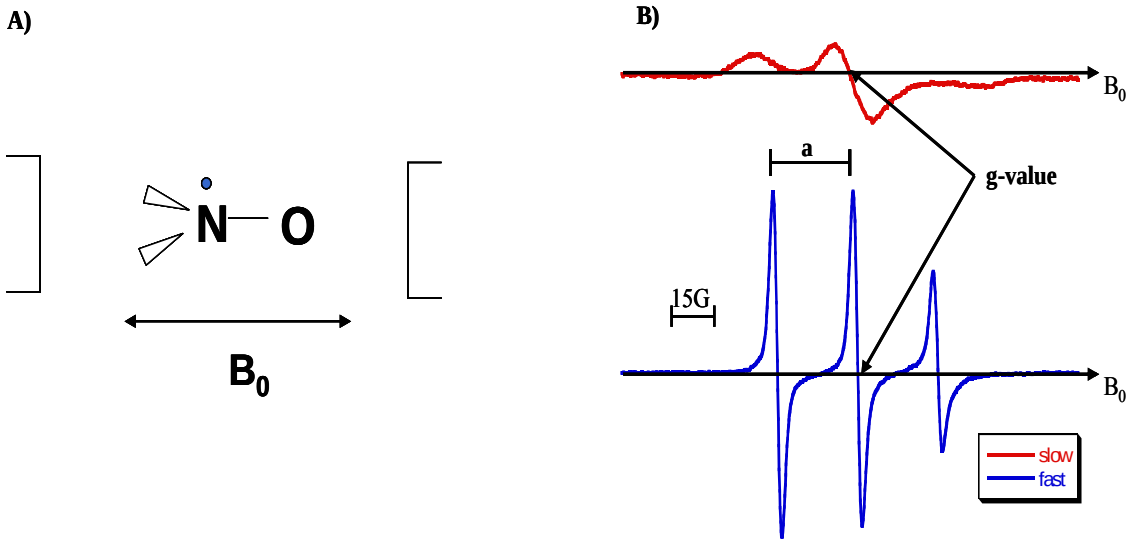

Figure 1-8: Monitoring dynamic motion of nitroxide radials *via* EPR spectroscopy. A) A diagram of the EPR instrumentation showing one orientation of the nitroxide radical in a magnetic field. B) A representative EPR spectra of nitroxide spin-probes with slow (red) and fast (blue) motion.

SDSL studies have been performed on a variety of RNA systems including model oligonucleotides (Qin et al. 2003, Kim et al. 2004), hammerhead ribozymes (Edwards and Sigurdsson 2005, Kim et al. 2005) and transactivation responsive (TAR) RNA-Tat peptide complexes (Edwards et al. 2001a, Edwards et al. 2001b). After attachment of select spin-label probes EPR spectroscopy can be used to monitor dynamics and structural characteristics. For example, the molecular motion of nitroxide side-chains can provide information about backbone dynamics and conformational changes. Different positions of the spin-label within the sequence may differ in solvent accessibility which identifies structural aspects and features of folding. Direct structural data is found by measuring the interspin distance between nitroxides or a nitroxide and other paramagnetic sources.

The distance between two paramagnetic centers can be obtained by measuring the dipolar electron spin-spin coupling (Rabenstein and Shin 1995, Sigurdsson and Eckstein 1996, Schiemann et al. 2003, Pham et al. 2004, Schiemann et al. 2004,). Figure 1-9 depicts site specific attachment of a spin-label within a single-stranded RNA. When two spin-probes are attached the intermolecular distance (r_{ab}) can be measured. Continuous wave (CW) EPR is a conventional method used to measure distances between spin-label probes (Kim et al. 2004). However, CW EPR is limited to distances less than 25 Å. A method used for analyzing interspin distances from CW EPR line shapes using Fourier deconvolution has been developed (Rabenstein and Shin 1995). The method deconvolutes an interacting and a noninteracting spectrum by Fourier transformation and division, and fits the resulting broadening function using Gaussian functions. Fourier transforms of the Gaussian fits are then used to extract distances.

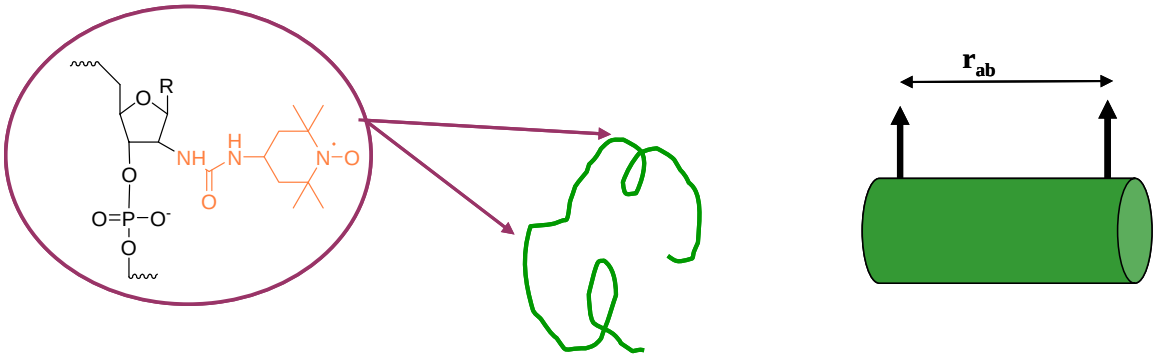

Figure 1-9: General overview of SDSL method. Spin-label probes are attached at finite positions within single-stranded RNA and the intermolecular distance (r_{ab}) of the nitroxide moieties can be measured.

Longer-range interactions of up to ~80 Å can be observed by pulsed electron-electron double resonance (PELDOR) (Schiemann et al. 2003, Bowmann et al. 2004, Schiemann et al. 2004,). Initial PELDOR RNA studies implemented the 4-isocyano TEMPO spin-label at 2'-amine modified U that forms a urea linkage within two short duplex systems (Schiemann et al. 2003). The distances obtained from this preliminary study were 35 and 63 Å which elaborate the distance range available for this

methodology (Schiemann et al. 2003). An analogous DNA PELDOR study was performed on a series of duplexes (12- 18-mer) (Schiemann et al. 2004). The spin-label, 2,2,5,5-tetramethyl-pyrrolin-1-yloxyl-3-acetylene (TPA), was attached to thymine (T) at varying internal sequence positions. The motivation for the TPA spin-label was its small and rigid structure which compared to 4-isocyano TEMPO, would reduce the distance distributions and gain a better correlation of the spin-spin distance with molecular modeling (Schiemann et al. 2004). The distances measured for DNA PELDOR study ranged from 19.2- 52.5 Å and aligned well with predictions from molecular dynamic simulations (Schiemann et al. 2004). PELDOR and other EPR spectroscopic techniques are more extensively described in the following reviews (Schweiger 2001, Jeschke 2003, Bennati and Prisner 2005).

Objectives

A previously published SDSL study from this laboratory investigated a 10-mer RNA duplex model system with spin-label probe succinimdyl-2,2,5,5-tetramethyl-3-pyrroline-1-oxyl-carboxylate (Kim et al. 2004). In this thesis a 4-isocyano TEMPO spin-label probe will replace the previously used succinimdyl-2,2,5,5-tetramethyl-3-pyrroline-1-oxyl-carboxylate in 10-mer SDSL studies. The influence of labeling with the 4-isocyano TEMPO spin-label in a 10-mer RNA model system will be investigated with thermal denaturation, Matrix Assisted Laser Desorption Time of Flight Mass Spectrometry (MALDI-TOF-MS), Electron Paramagnetic Resonance (EPR) spectroscopy, and reverse phase high performance liquid chromatography (RP-HPLC).

In the 10-mer RNA duplex model system a 4-isocyano TEMPO spin-label is individually attached to one strand and two strands are annealed to measure distances. This methodology is limited to systems in which two oligonucleotides are annealed together. To circumvent this limitation and also to explore single-strand dynamics, a new methodology was implemented and termed double spin-labeling. Double spin-labeled single-stranded RNA will be investigated as a single-strand and within a duplex *via* MALDI-TOF-MS, EPR spectroscopy and RP-HPLC. A double spin-labeling strategy developed in this work will be applicable to large complex RNAs like the Group I intron of *Tetrahymena thermophilia*.

CHAPTER II
MATERIALS AND METHODS

RNA deprotection and purification

The 10-mer RNA sequences used in this research were purchased from Dharmacon Research (Lafayette, CO) and they were synthesized by solid-phase methods. The specific sequences used are named U6 and U7 and this nomenclature denotes the position from the 5'-end for the site of modification on uridine as was used in previous research within this laboratory (Figure 2-1) (Kim et al. 2004). In addition, modified (mod) sequences U6mod, U62mod and U7mod, where mod indicates 2'-NH_2 substitution of the 2'-OH on the ribose sugar of select nucleotides within RNA sequences were also obtained (Figure 2-1). The amine modification(s) are required to facilitate the attachment of spin-label probes. These modifications are currently available with uridine and cytosine; however in this work only uridine modifications were employed. In the latter part of this research two 2'-NH_2 modifications were made in the U6 sequence, one at the original site, U6, and another at position 3. This sequence was termed U62mod. It should also be noted that U6 and U7 are complimentary 10-mer strands that were studied in duplex and also as single-strands.

U6 sequences

Wild type	5' CCUAGUGUGG 3'
U6mod	5' CCUAG**U**GUGG 3'
U62mod	5' CC**U**AG**U**GUGG 3'

U7 sequences

Wild type	3' GGAUCACACC 5'
U7mod	3' GGA**U**CACACC 5'

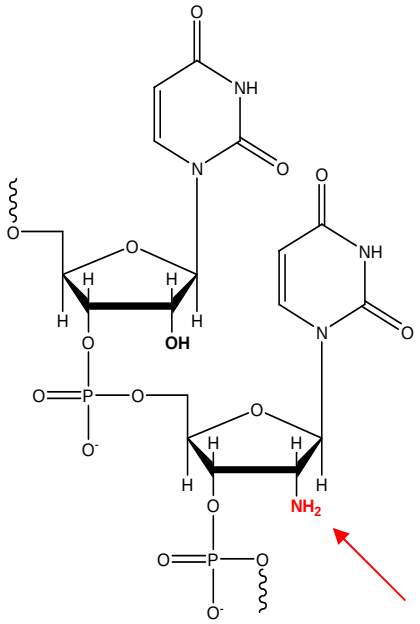

Figure 2-1: 10-mer RNA sequences used in this research. A modification (mod) indicates a 2'-NH_2 substitution on the ribose sugar as depicted by the arrow. Modification at select uridine positions is denoted in red.

The RNAs were shipped as a pellet and protected at the 2' position with a 2'-ACE® protecting group, as shown in Scheme 1. Deprotection was performed as outlined by the manufacturer as depicted in Scheme 1. 400 µL of provided 100 mM acetic acid deprotection buffer, titrated to pH 3.8 with N,N,N',N'-Tetramethylethylenediamine (TEMED), was added to the RNA pellet and the solution was pipette mixed, vortexed and centrifuged. The solution was then incubated in a 60 ^{0}C water bath for a minimum of 30 minutes. After deprotection and incubation, a 1:1 volume ratio of Ambion (Austin, TX) loading buffer was added to the solution. The loading buffer contained formamide and molecular weight markers (bromophenol blue and xylene) for visualization during subsequent gel electrophoresis. Purification of RNA was performed using denaturing gels (3 mm thickness, 20% polyacrylamide, 7 M urea) and 1 X Tris- Borate- EDTA (TBE) running buffer (Tris Hydroxymethylaminoethane (Tris)/ boric acid (BA)/ ethylenediaminetetraacetic acid (EDTA)) , applying 250 V for ~ 4 hours.

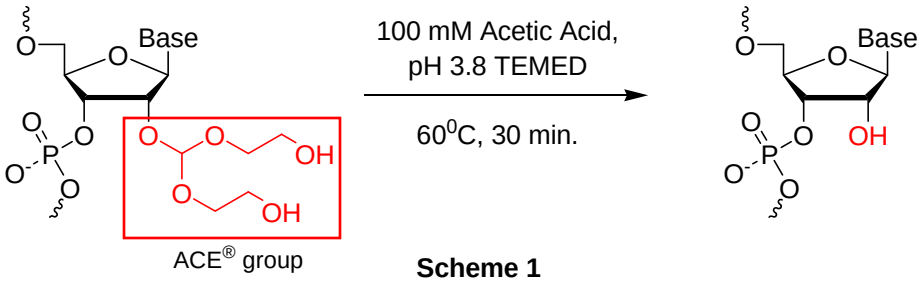

Scheme 1

UV shadowing was implemented for visualization of RNA bands in the gel which were then excised. Select gel bands were further sliced with a clean razorblade into smaller fragments and placed into a Falcon tube with 5 mL of gel elution buffer (0.2 % sodium dodecyl sulfate (SDS), 5 mM triethanolamine (TEA), pH 7.8, 250 mM NaCl). The Falcon tubes were then placed in a shaker set at 37 ^{0}C and 300 rpm, and the elution buffer volume was refreshed (V_t was removed, stored and additional 5 mL was added) over a minimum of a 36 hour period. UV shadowing of the gel fragments was performed after each refreshed volume to ensure RNA elution. All aliquots were combined and an organic phase extraction was performed with an equal volume of a phenol: chloroform: isoamyl alcohol (25:24:1) (Ambion) solution. This was followed by an additional organic phase extraction in an equal volume ratio (3X total) with chloroform: isoamyl alcohol (24:1) solution, to extract SDS and chloroform.

The aqueous RNA solution was then concentrated using Centricon YM-3 (Amicon- Millipore) tubes and centrifugation at 6500 rpm. The Centricon YM-3 tubes required filter preparation with a 2 mL volume of water flushed through (6500 rpm), and then the samples were added and buffer exchanged (V_t = 4 mL) with 5 mM TEA, pH 7.8, 100 mM NaCl. Ethanol precipitation was performed by adding 1/10th volume 3 M sodium acetate (NaOAc), 3X volume ethanol (EtOH), 2 µL glycogen to the RNA solution in an Eppendorf tube and incubating at -30 ^{0}C overnight. The Eppendorf tube was then placed in a centrifuge at 4 ^{0}C, centrifugated at 14000 rpm for 30 minutes and then the ethanol supernatant was removed. The subsequent RNA pellet was dried in a

Jouan vacuum concentrator, washed with ~100 μL 70% EtOH and resuspended in a 70 mM Boric Acid (BA), pH 8.6 solution.

RNA concentrations were determined by monitoring absorbance at 260 nm with a Cary 300 Bio UV-VIS spectrometer. The extinction coefficients for all U6 (97,200 L/ mol · cm) and U7 (96,400 L/ mol · cm) derived sequences were supplied by Dharmacon. A quartz cell containing a minimum of 500 μL dd H_2O was used to obtain a background spectrum that scanned 500- 200 nm. The quartz cell was removed and a minimum of 1 μL of RNA solution was added to the dd H_2O within the quartz cell, and was pipette-mixed. The quartz cell was then inserted within the spectrometer and absorbance values were obtained. The concentration was calculated based on the maximum absorbance (λ = 260 nm). Purified RNA sequences were stored at -30 ^{0}C freezer until later use.

Synthesis of 4- isocyano TEMPO spin-label

4-Isocyano-2,2,6,6-tetramethylpiperidinooxy (TEMPO) was used as a spin-label probe for Site-Directed Spin-Labeling (SDSL) studies in RNA systems (Edwards et al. 2001). The synthetic route employed in this research for the desired 4-isocyano TEMPO spin-label is depicted in Scheme 2. This procedure was adapted from a previously published method (Sigurdsson et al. 1996). Modifications to the previously published procedure were made to include the incorporation of user-friendly triphosgene instead of diphosgene (Sigurdsson et al. 1996). Also, acid (HCl) and base (NaOH) aqueous extractions were replaced with a single neutral aqueous extraction with doubly-deionized water. This modified procedure achieved an isolated 70% product yield based on the starting material compared to a previously published 39% yield, both values based upon 100% conversion (Sigurdsson et al. 1996).

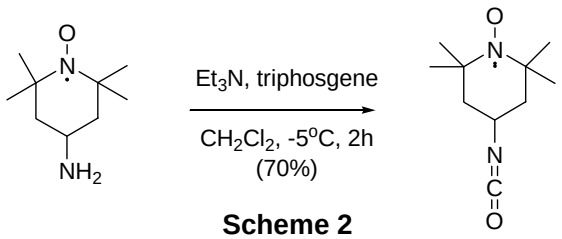

Scheme 2

The chemicals used in the synthesis include 4-amino TEMPO which was purchased as a solid from Fisher Scientific, triphosgene which was purchased as a solid from Acros Organics, TEA and CH_2Cl_2 which were freshly distilled from calcium hydride in Dr. Daniel Romo's laboratory. It was essential to handle each substance with caution as they could readily hydrolyze releasing corrosive products if not handled properly. 4-amino TEMPO and triphosgene were stored at -20 ^{0}C however when in use it was imperative to let the TEMPO slowly warm to room temperature before performing the spin-labeling reaction. Also, great caution was taken with the triphosgene as prolonged air exposure can cause the substance to decompose, therefore before returning to the freezer for storage the container was placed under a blanket of nitrogen, promptly sealed and covered with Parafilm®. Through the duration of the synthesis investigation it was found that freshly distilled TEA and CH_2Cl_2 out-performed stored chemicals.

After a variety of factors were modified, this general synthetic route was used to generate 4-isocyano TEMPO. The experimental setup is schematized in Figure 2-2. The mass measurements and the reaction were carried out in the hood. First, 4-amino TEMPO was removed from the freezer and allowed to warm to room temperature. While this occurred, two dry (washed, ovendried and then stored in a dessicator) 10 mL round-bottom flasks (RBFs) were weighed. On average 200 mg of 4-amino TEMPO was added to one RBF, with stirbar and septum. A Schlenk line with N_2 flow secured an immersed RBF in an ice bath on a stirplate. The stock 4-amino TEMPO was then returned for storage and the triphosgene was taken out. A 3:1 molar ratio of 4-amino TEMPO to triphosgene dictated the mass of triphosgene added to the second RBF (~ 0.08 g) triphosgene. The second RBF with stirbar and septum was immersed in the icebath and then secured to the Schlenk line under N_2. The excess triphosgene container was blanketed with nitrogen, sealed, wrapped in Parafilm® and returned for storage.

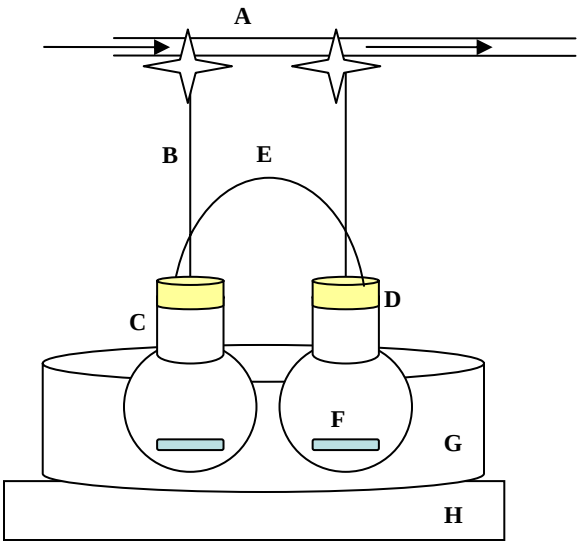

Figure 2-2: Schematic of the experimental setup used for the synthesis of 4-isocynao TEMPO. (A) represents a Schlenk line showing the direction of N_2 gas flow. (B) represents the rubber tubing connection from the Schlenk line to 2 RBFs (C) with needles through septa (D) to continue the N_2 flow. (E) is the cannula used to transfer solutions from one RBF to another. (F) are the stirbars within the RBF used to mix the solutions. (G) is the ice water bath housed on top of the stir plate (H).

A 5mL syringe (fresh for each reaction) was used to procure freshly distilled CH_2Cl_2. 2.5 mL of dichloromethane was added to the 4-amino TEMPO RBF and then to the triphosgene RBF. The two RBFs were stirred to dissolve the solids in CH_2Cl_2. A cannula was then linked to each RBF through the septa while the compounds dissolved. A second 1 mL syringe (fresh for each reaction) was used to procure freshly distilled TEA. The 4-amino TEMPO solution was cannula transferred followed by TEA addition to the triphosgene-containing RBF. The reaction proceeded for 10 minutes in an icebath (**G**) and (**G**) was then removed while the RBF is still attached to the Schlenk line and continued to stir. The reaction was continued for an additional 3.5 hours at room temperature.

After 3.5 hours, freshly distilled CH_2Cl_2 was added to the reaction mixture (V_t = 20 mL) and the mixture was stirred while under the Schlenk line. The reaction vessel was then removed and the volume transferred to a 50 mL separatory funnel containing 5 mL of autoclaved doubly deionized (dd) Milli-Q water as an aqueous workup. The

separatory funnel was stoppered, shaken and Na_2SO_4 was then added to dry the organic phase. The dichloromethane solution (organic phase) was then transferred to a new dry RBF, concentrated *en vacuo* and the obtained orange crystalline solid was stored at -30 ^{0}C until needed for subsequent spin-labeling reactions.

Confirmation of the desired 4-isocyano TEMPO product was achieved through ^{1}H NMR spectroscopy, electrospray ionization time-of-flight mass spectrometry (ESI-TOF-MS), and Infared (IR) spectroscopy. ^{1}H NMR spectra were obtained on 300 MHz instruments (Mercury 300 and Inova 300), with $CDCl_3$ as the solvent. Figure 2-3 depicts the structures of diagnostic methine peaks that were monitored with ^{1}H NMR during the spin-labeling reaction which are urea (**A**), isocyanate (**B**) and amine (**C**) as described previously (Edwards et al. 2001a).

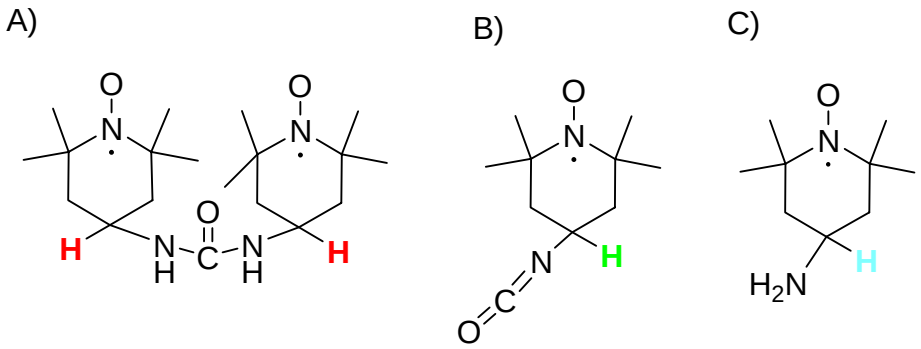

Figure 2-3: Structures of diagnostic methine protons. A) urea-linked bis-TEMPO, B) 4-isocyano TEMPO, and C) 4-amino TEMPO structures. The methine proton is highlighted in red within (A), green within (B), and blue within (C) which is the diagnostic ^{1}H monitored during the spin-labeling reaction.

Aliquots (0.1 mL) were taken to monitor the spin-label synthesis reaction via ^{1}H NMR to avoid the production of the urea complex. Figure 2-4 is a representative ^{1}H NMR spectrum that observed the presence of (A), (B), and (C) during the synthesis of 4-isocyano TEMPO. The ^{1}H NMR spectrum for an aliquot of the reaction after 45 minutes is shown in Figure 2-5. 4-Amino TEMPO and competing base TEA are the starting materials (^{1}H signals at 3.4 and 3.1 ppm respectively), which generated the 4-isocyano

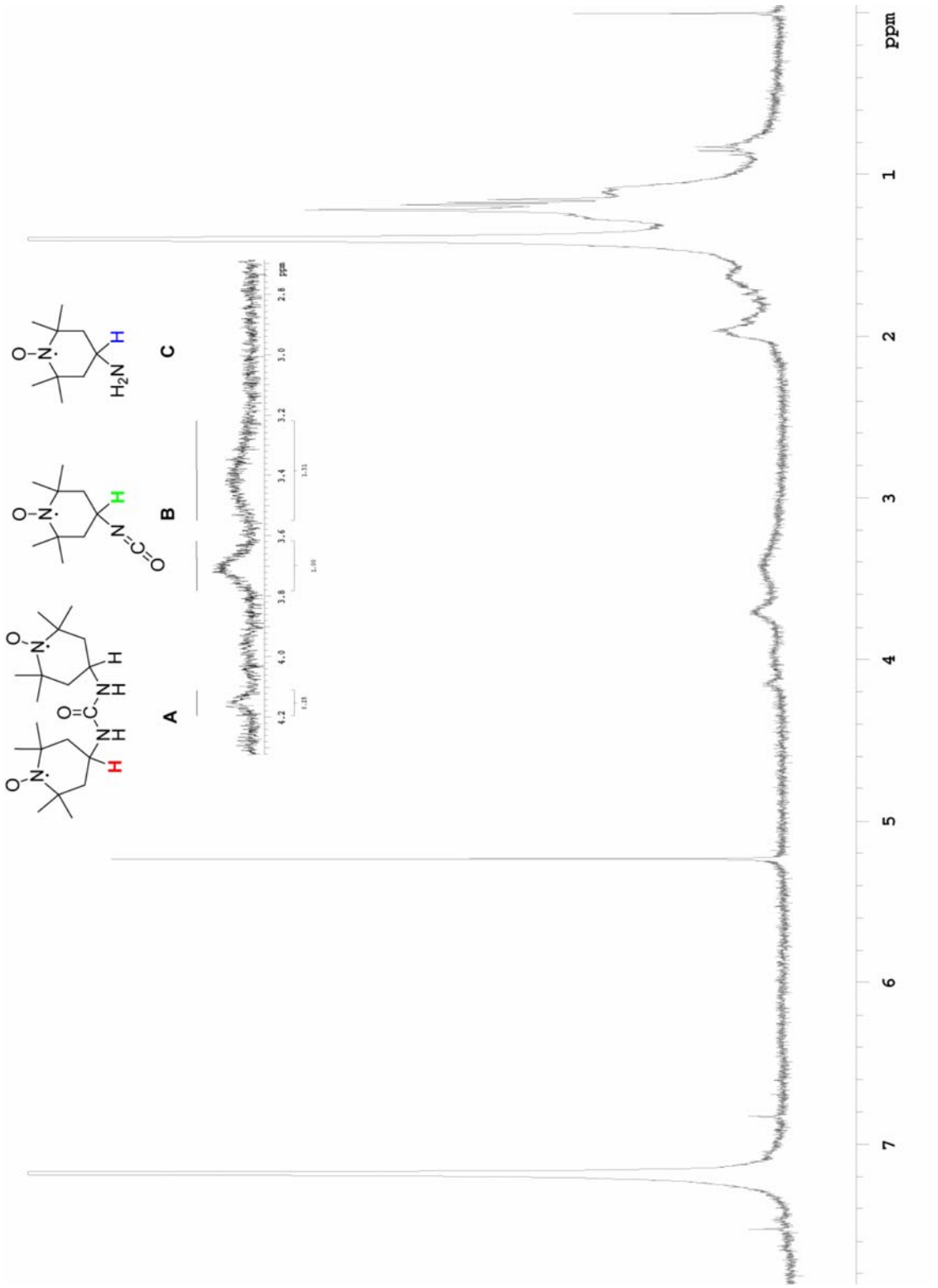

Figure 2-4: Representative ^{1}H NMR spectrum obtained on a 300 MHz instrument showing diagnostic methine peaks observed during the synthesis of 4-isocyano TEMPO. Urea (**A**), isocyanate (**B**) and amine (**C**) methine structures are positioned above corresponding peaks.

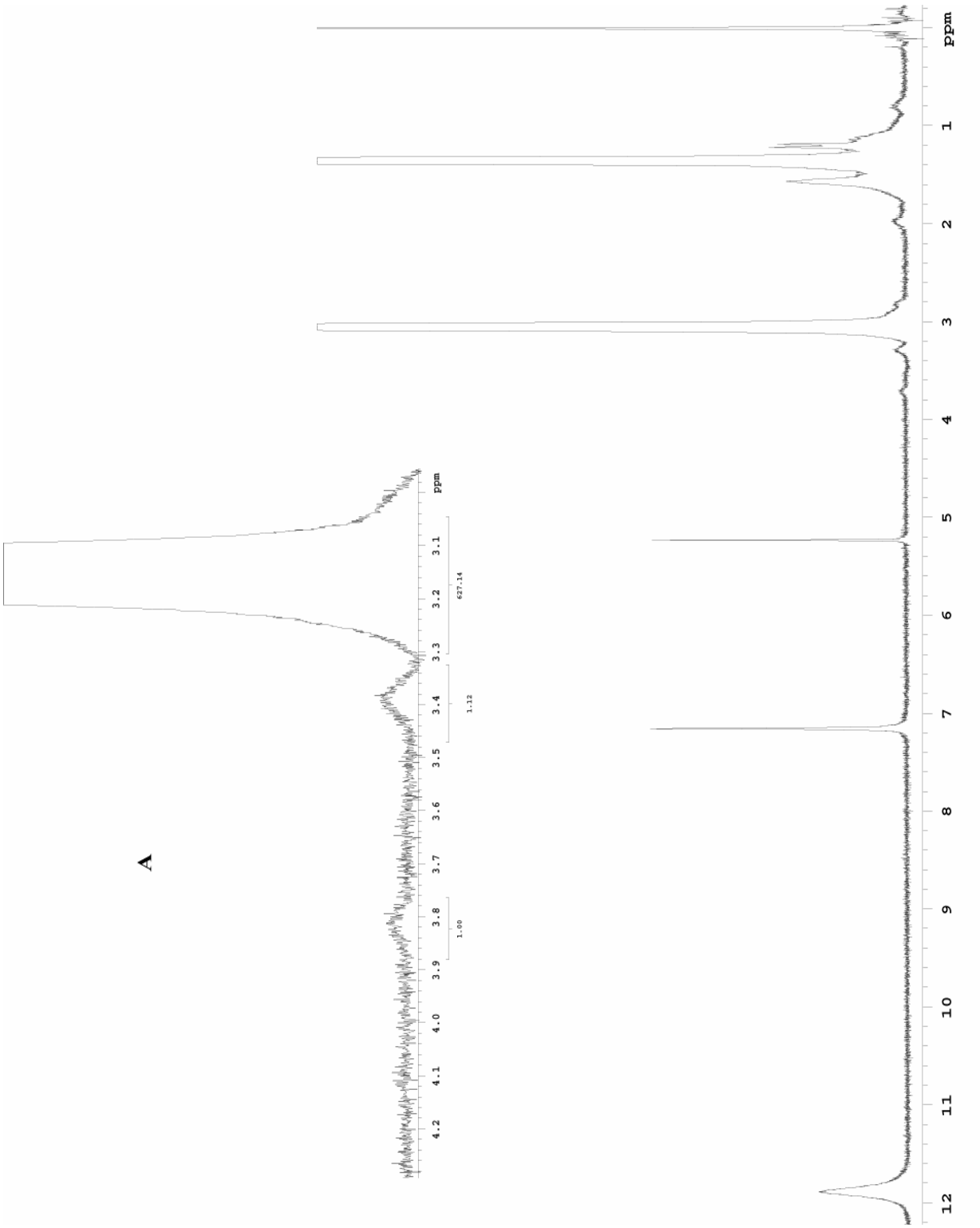

Figure 2-5: ^{1}H NMR of 4-isocyano TEMPO spin-label synthesis aliquot after 45 minutes of reaction. (**A**) is an inset highlighting product formation (3.8 ppm), starting materials 4-amino TEMPO and TEA at 3.4 and 3.1 ppm respectively.

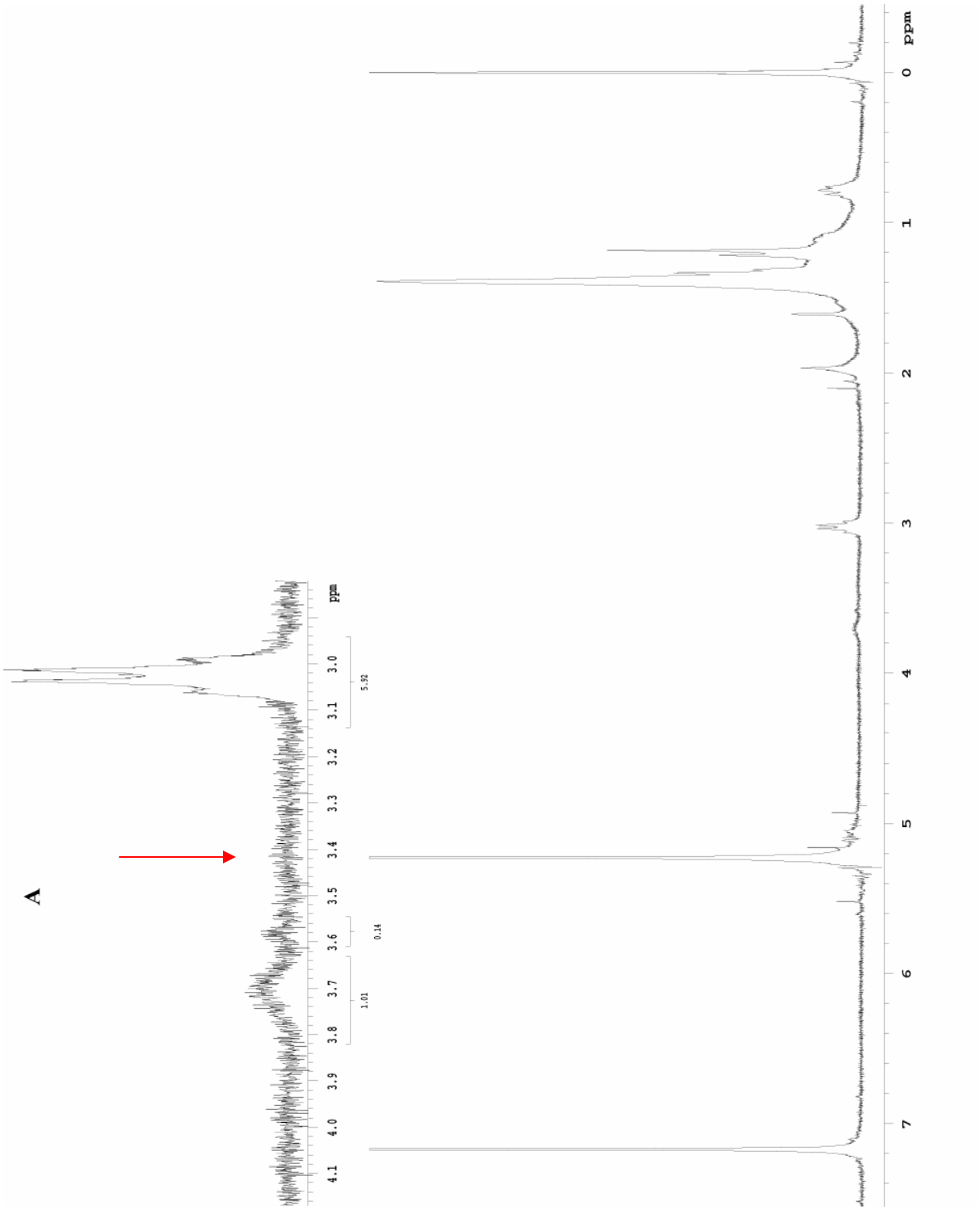

Figure 2-6: ^{1}H NMR of 4-isocyano TEMPO spin-label synthesis aliquot after 2 hours of reaction time. (**A**) is an inset highlighting product formation (3.8 ppm), and starting material TEA at 3.1 ppm. After 2 hours 100 % conversion was achieved (the arrow denotes loss of 4-amino TEMPO starting material).

TEMPO product (3.7 ppm). As the reaction progresses the starting materials are consumed and 4-isocyano TEMPO was produced to capacity (Figures 2-5 and 2-6). A competing reaction is the formation of urea-linked bis-TEMPO product. This undesired product can be monitored *via* its urea proton signal at 4.2 ppm. Order of addition and temperature parameters minimized the production of urea-linked di-TEMPO product.

Mass spectrometry (MS) was also employed to confirm the synthesis of 4-isocyano TEMPO. An aliquot of the reaction mixture was used for MS analysis. 1 mL of the reaction mixture was concentrated *en vacuo* and submitted to the Laboratory of Biological Mass Spectrometry (LBMS). Figure 2-7 is a representative positive-ion mode ESI-TOF-MS spectrum which was indicative of 4-isocyano TEMPO spin-label with a molecular ion at 198 mass units. Further, IR spectroscopy showed an NCO stretch at 2270 cm^{-1} which also substantiated spin-label synthesis (data not shown).

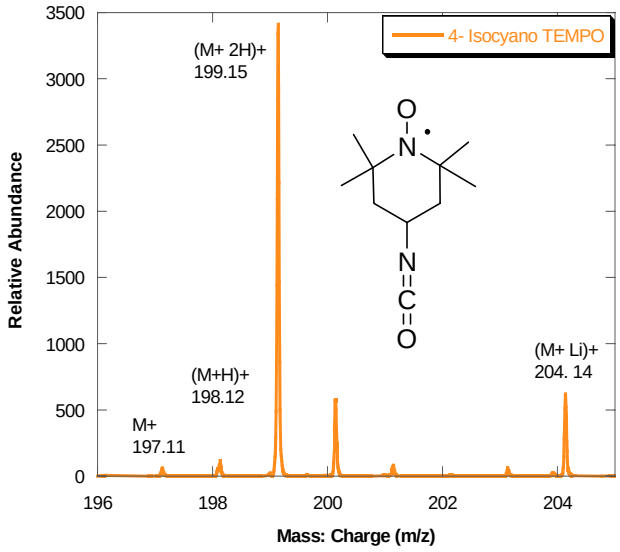

Figure 2-7: ESI-TOF-MS spectrum of 4-isocyano TEMPO reaction mixture. The molecular weight of the spin label is 197 mass units. Positive-ion mode ESI-TOF-MS showed the diagnostic molecular ion at 198 in addition to the Li^+ adduct that was also observed.

Spin-labeling reaction

The 2'-NH_2 modified RNA sequences (U6mod, U62mod and U7mod) were spin-labeled with 4-isocyano TEMPO as outlined by previously published work and depicted in Scheme 2 (Edwards et al. 2001a). Small deviations from the published procedure included an increase in the spin-label concentration (75 to 300 mM), an increase in the reaction time (1 to 2 hours minimum) and temperature environment (-8 ^{0}C to 5 ^{0}C water bath).

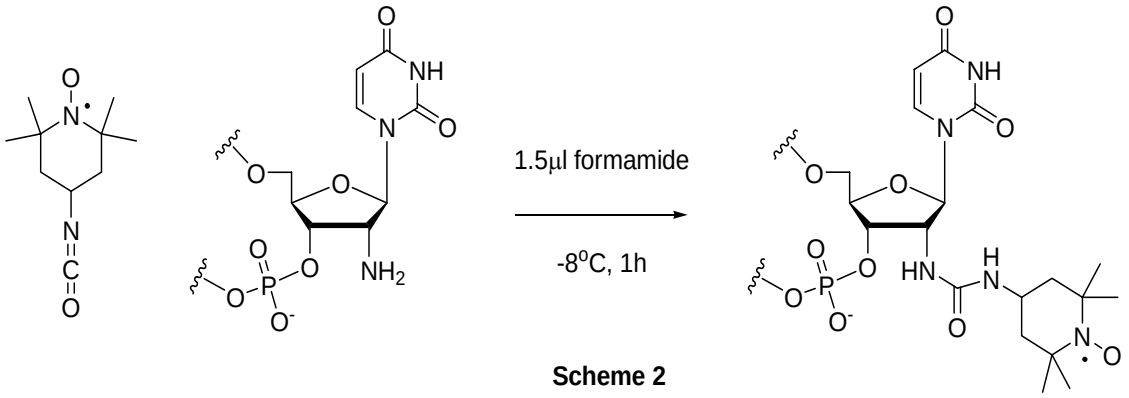

Scheme 2

The spin-labeling reaction procedure is detailed as follows. The 4- isocyano TEMPO stock sample was removed from the -30 ^{0}C freezer and warmed to room temperature. Next, a 300 mM solution of spin-label in DMF was prepared by measuring the mass of the spin-label and dissolving it in dimethyl formamide (DMF). A 10 µL spin-label stock solution was prepared in an Eppendorf tube, but caution was used as exposure to water (in the DMF) can degrade the spinlabel. An increased concentration (300 mM) was implemented due to possible impurities present in this synthesized 4-isocyano TEMPO.

The spin-labeling reaction vessel used in these experiments was a 70 µL Eppendorf tube placed in a Styrofoam ice-water bath (prepared in advance). The 2'-NH_2 modified RNA sequences are stored in 70 mM BA, pH 8.6 at -30 ^{0}C until needed for spin-labeling reactions. A 5 nmole reaction scale was used which required 2.5 µL of 2

mM RNA in 70 mM BA, pH 8.6, was added to 1.5 μL formamide in the Eppendorf tube. 1μL of the 300 mM spin-label (DMF) stock was transferred to the 70 μL Eppendorf tube. The reaction solution was then pipette mixed, vortexed, centrifuged and then placed within Styrofoam ice-water bath. The Styrofoam ice-bath was then transferred to the cold room (5 ^{0}C) and the reaction proceeded for a minimum of 1 hour time. Optimization conditions for the spin-labeling the U62mod sequence have not been obtained however when using an increased amount of RNA the ratio of all components was increased by the same factor. The spin-label concentration, temperature of the reaction and reaction time are variables that may contribute to the conversion efficiency of the spin-labeling reaction.

The Eppendorf reaction vessel was then removed and 20 μL of dd H_2O was added to the Eppendorf tube. Chloroform was added (600 μL) to the solution which was then vortexed and centrifuged. The organic layer was removed and additional organic extractions (5 X total) with chloroform were performed to remove un-reacted spin-label. The washed aqueous solution was then ethanol precipitated overnight following addition of 1/10th volume NaOAc, 3X volume EtOH and 2 μL glycogen. The ethanol precipitation procedure as previously outlined was followed and the spin-labeled RNA was resuspended in ~ 20 μL of 5 mM TEA, pH 7.8, 100 mM NaCl. The concentration that resulted from the addition of buffer was not measured. Further procedures were generally based on using a total number of nmoles of RNA, and so this exact concentration is not critical. Spin-labeled RNA samples were stored at -30 ^{0}C freezer until later use.

Confirmation and purification of spin-labeled RNA

After the spin-labeling reaction was completed (followed by workup and proper storage), MS was implemented to confirm formation of the covalent urea linker depicted in Scheme 2. Matrix Assisted Laser Desorption Ionization Time of Flight (MALDI-TOF)-MS sample submission requires ~1 nmole of the spin-labeled RNA mixture in minimal (V_t < 3 μL) doubly deionized (dd) autoclaved water. After the spin-labeling reaction the labeled RNA was stored in 5 mM TEA, pH 7.6, 100 mM NaCl. These buffer conditions are required for subsequent EPR procedures but are not compatible for MS

therefore buffer exchange and concentration was performed with a Centricon YM-3. It is critical to exchange sodium and TEA counterions with more volatile ammonium ions for the matrixes used in MALDI-TOF-MS.

Initially the Centricon filter was conditioned with 2mL of dd water which was followed by two additions (V_t = 4mL) of 100 mg/ mL diammonium citrate (Fisher) in water with a centrifugation of 6500 rpm. After the filter was conditioned, the RNA spin-labeled solution (in 5 mM TEA, pH 7.8, 100 mM NaCl) was added to the Centricon tube to buffer exchange and concentrate. Two buffer exchanges (V_t = 4 mL) of 100 mg/ mL diammonium citrate were followed by two additions (V_t = 4 mL) of 10 mg/ mL diammonium citrate. The volume was concentrated to ~300 μL with the Centricon tube and then transferred to a Jouan RC 10.22 vacuum concentrator in an Eppendorf tube and dried to pellet form. The pellet was then resuspended in minimal (~ 2 μL) autoclaved dd water and the solution submitted for MS analysis by the LBMS. Typical MS traces are shown in Chapters III & IV.

Upon confirmation of spin-label attachment, Reverse-Phase High Performance Liquid Chromatography (RP-HPLC) was implemented to purify the spin-labeled from the non spin-labeled RNA. RP-HPLC takes advantage of differences in polarity within this mixture which promote separation. Specifically, the 2'-NH_2 modified RNA elutes faster than the spin-labeled RNA (Edwards et al. 2001a). The HPLC methodology used in this work is based largely upon a previously published procedure (Edwards et al. 2001a, Kim et al. 2004).

A Sephasil^{TM} Peptide C_{18}, 5 μL, ST 4.6/ 250 column (Pharmacia Biotech) was used on an Amersham Biosciences HPLC instrument implementing a UV detector used to monitor the RNA elution at 260 nm. Unicorn 4.11 software was used to implement the following HPLC method. An HPLC gradient used two buffers to separate spin-labeled from nonspin-labeled RNA. Buffer A contained 50 mM Et_3NH, 5mL acetic acid (AcOH), pH 7.6 in a water. Buffer B contained 30% Buffer A and 70% acetonitrile (ACN) volume ratio. All buffer solutions were made with dd water, filtered and degassed (1 hour with N_2). The HPLC column was then flushed for ~20 minutes, 0.5 mL/ min, with a 50% gradient containing Buffer A and B to remove storage buffer from the column. RNA samples containing a minimum of 5 nmoles and a maximum of 40 nmoles were

dissolved in 300 μL dd H_2O prepared in Eppendorf tubes and syringe injected into the HPLC. The HPLC method contained 3 column volumes (CV) 100% Buffer A, a 1 CV ramp to 11% Buffer B, a 6 CV gradient from 11-23% B, a 1 CV ramp to 100% B followed by 1 CV 100% B with a 0.5 mL/ min flow rate. Fractions (0.5 mL) were collected during the 11-23% gradient period. Representative RP-HPLC traces are shown in Chapters III & IV.

Regions of elution were determined for the spin-labeled RNA as separated from the non-labeled RNA and the corresponding fractions were combined. The volume from each region of the fractions was reduced on a Jouan RC 10.22 Speed-Vac. 4 mL of dd water was added to the culture tube and concentrated. RP-HPLC fractions are prepared differently for MS analysis in comparison to Electron Paramagnetic Resonance (EPR) spectroscopy. In MS samples these fractions were not concentrated directly with Centricon tubes because the ACN can destroy the filter. After a minimum of 4 mL of autoclaved dd water was added to the fractions and reduced, the solution was then transferred to Centricon YM-3 tubes (filter treated prior to use) when required for MS analysis. MALDI-TOF-MS samples of HPLC fractions followed the MS protocol outlined previously. When the RNA sample was used for EPR it was dried to a pellet, resuspended in 5 mM TEA, pH 7.6, 100 mM NaCl and stored at -20 ^{0}C.

Thermal denaturation

UV-Vis thermal denaturation was implemented to monitor secondary structure stability of 10-mer RNA duplexes. This biophysical method primarily determines the melting temperature, T_m. Thermal denaturation profiles were obtained by plotting the derivative of absorbance (dA/dT) as a function of increasing temperature.

A Cary 300 double beam UV-Vis spectrometer equipped with a 6 cell block and variable temperature controller was implemented to monitor thermal denaturation profiles. Samples were prepared as 2 μM RNA duplexes in 900μL of 5mM TEA buffer, pH 7.8, 100mM NaCl, which were annealed at 90 ^{0}C for 90 seconds on a heating block and then placed in ice to cool for 30 minutes. The cooled duplex solution was then transferred to quartz cuvettes that were sealed at room temperature. The cuvettes were then inserted into the spectrometer and equilibrated at 5 ^{0}C for 10 minutes. One cuvette containing

only reference buffer was used to house the temperature probe within the spectrometer. The temperature was increased with a rate of 0.3 ^{0}C/ min from 5 to 90 ^{0}C, which was monitored by the temperature probe and data points were taken at each interval. Absorbance at 260 and 280 nm was measured as a function of increased temperature.

EPR spectroscopy

Diagnostic room temperature (RT) EPR measurements were taken with 20 μL samples in 5 mM TEA, pH 7.6, 100 mM NaCl. RT and Low Temperature (LT) EPR samples were initially prepared in Eppendorf tubes and then pipette-transferred to capillary tubes (Kimble Glass Inc.). After EPR spectra were collected the 20 μL samples were recovered and stored at -30 ^{0}C. Low temperature (LT) EPR samples were prepared in a 70 μL volume containing 29 μM RNA, 5 mM TEA, pH 7.6, 100 mM NaCl, 20 % ethylene glycol. The cryoprotectant, ethylene glycol, was added to the Eppendorf tube containing an RNA solution which was pipette-mixed and transferred to the capillary tube. In a duplex sample 2 nmoles of each strand (5 mM TEA, pH 7.6, 100 mM NaCl) are annealed (90 seconds at 90 ^{0}C on a heating block, cooled on ice 30 minutes) followed by the addition of the cryoprotectant in the same manner described above.

X-band EPR measurements were obtained using a Bruker ESP 300 spectrometer with a TE_{102} cavity, an Oxford Instruments liquid helium/nitrogen cryostat, an HP 5352B microwave frequency counter, and a Bruker ER 041XG microwave bridge (Samples et al. 2005). The instrument is capable of recording EPR spectra at room temperature and 273 K to 90 K (using liquid nitrogen), and 90 K to 4 K (using liquid helium). Only two temperatures were used in this research, room temperature and 100K for LT measurements. EPR spectra were collected at 100 K with 5 scans over a sweep width of 150 G with a microwave power of 5 mW, 0.80 G magnetic field modulation amplitude at a frequency of 100 kHz, time constant of 328 ms and sweep time of 168 s. Bruker software was used to gather and manipulate data, in addition to WIN EPR and Kaliedagraph 3.6 for displaying data.

Molecular modeling

Intermolecular distance between the nitroxide moieties in an RNA oligonucleotide were determined with computer simulations as outlined by previously published (Kim et al. 2004). Using UNIX-based Insight II, the Biopolymer module was used to construct an A-form RNA duplex with 4-isocyano TEMPO spin-label attached to designated positions (Accelrys Software Inc.). Energy minimizations and molecular dynamic (MD) calculations were performed using the Discover 3 module within this suite.

CHAPTER III
COMPARISON OF UREA- AND AMIDE-LINKED SPIN-LABELS IN A 10-MER RNA MODEL SYSTEM

Background and motivation

A previous SDSL study was performed on a series of 10-mer RNA sequences which implemented succinimdyl-2,2,5,5-tetramethyl-3-pyrroline-1-oxyl-carboxylate (**1**) as the spin-label probe (Kim et al. 2004). Spin-label attachment is facilitated through 2'-amine modifications in specified RNA nucleotides (Edwards et al. 2001a). Upon spin-labeling at select uridine nucleotides a resulting bond formation, "linker", is generated at the 2' position. As shown in Figure 3-1, when (**1**) is used as the spin-label probe an amide linker (**A**) is generated (Kim et al. 2004). However, increased spin-labeling efficiency in RNA is observed with an isocyanate derivative of tetramethylpiperidyl-N-oxy (TEMPO) **(2)** (Edwards et al. 2001a). Further, when **(2)** is used as a spin-label probe a urea linker (**B**) is generated (Edwards et al. 2001a).

The 10-mer sequences studied by Kim and coworkers are shown in Table 3-1 (Kim et al. 2004). A subset of these sequences, specifically U6 and U7 were spin-labeled with **(2)** in this research. The spin-label probe in (**A**) has a smaller ring size and shorter linker length compared to that derived from (**2**). The potential influence of the spin-probes, with respect to size and linker length differences, in molecular dynamics and distance measurements is a primary objective in this study. It is suggested that the longer linker will allow the nitroxide probe to rotate more freely which could be advantageous.

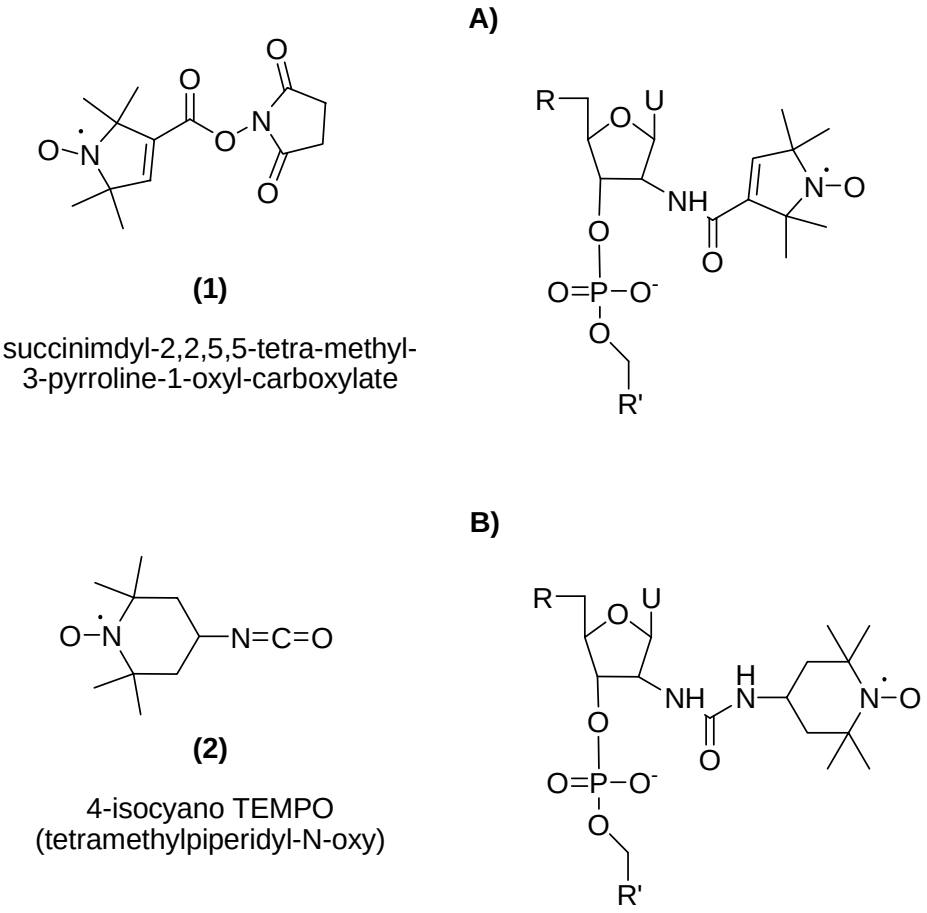

Figure 3-1: Nitroxide spin-label probes **(1)** and **(2)** used for SDSL studies. When **(1)** was implemented an amide linker between ribose and the spin-label is obtained (Kim et al. 2004), while when **(2)** is implemented a urea linker is formed (Edwards et al. 2001a).

Table 3-1: 10-mer RNA sequences used in SDSL studies (Kim et al. 2004).

Name		10-mer Sequence	
U3	5'	C C U A G U G U G G	3'
U5	5'	C C U A U G G U G G	3'
U6	5'	C C U A G U G U G G	3'
U7	5'	C C A C A C U A G G	3'
U7A	5'	C C A C C A U A G G	3'
U7B	5'	C C U A G G U U G G	3'
U7C	5'	C C A A C C U A G G	3'
U8	5'	C C U A G U G U G G	3'
U8A	5'	C G A U G U G U G C	3'
U8B	5'	G C A C A C A U C G	3'

Mass spectrometry of spin-labeled sequences

MALDI-TOF-MS was used to confirm the attachment of **(2)** to 2'-NH_2 modified positions within U6 and U7 sequences. Table 3-2 shows the molecular weight and predicted molecular ion for 2'-NH_2 modified and spin-labeled sequences. Initially, MALDI-TOF-MS spectra of 2'-NH_2 modified sequences were obtained. U6mod and U7mod molecular ions were observed in addition to their corresponding sodium and potassium adducts as shown in Figure 3-2. After conjugation with 4-isocyano TEMPO spin-label, additional MALDI-TOF-MS samples were prepared. As shown in Figure 3-2, C and D, the results confirmed the covalent attachment of the spin-label probe to sequences U6 and U7. The added spin-label probe linkage shifted the molecular ion by ~198 daltons. Sodium and potassium adducts were also seen in the spin-labeled samples. MALDI-TOF-MS was successfully implemented as a qualitative detection technique for spin-label probe attachment within each sequence.

Table 3-2: Molecular ions for 10-mer RNAs in MALDI-TOF-MS.

Name	MW	$(RNA)^+$	MW (RNA + SL)	$(RNA + Spinlabel)^+$
U6 mod	3175.9	3176.9	3373.1	3374.1
U7 mod	3141.9	3142.9	3339.1	3340.1

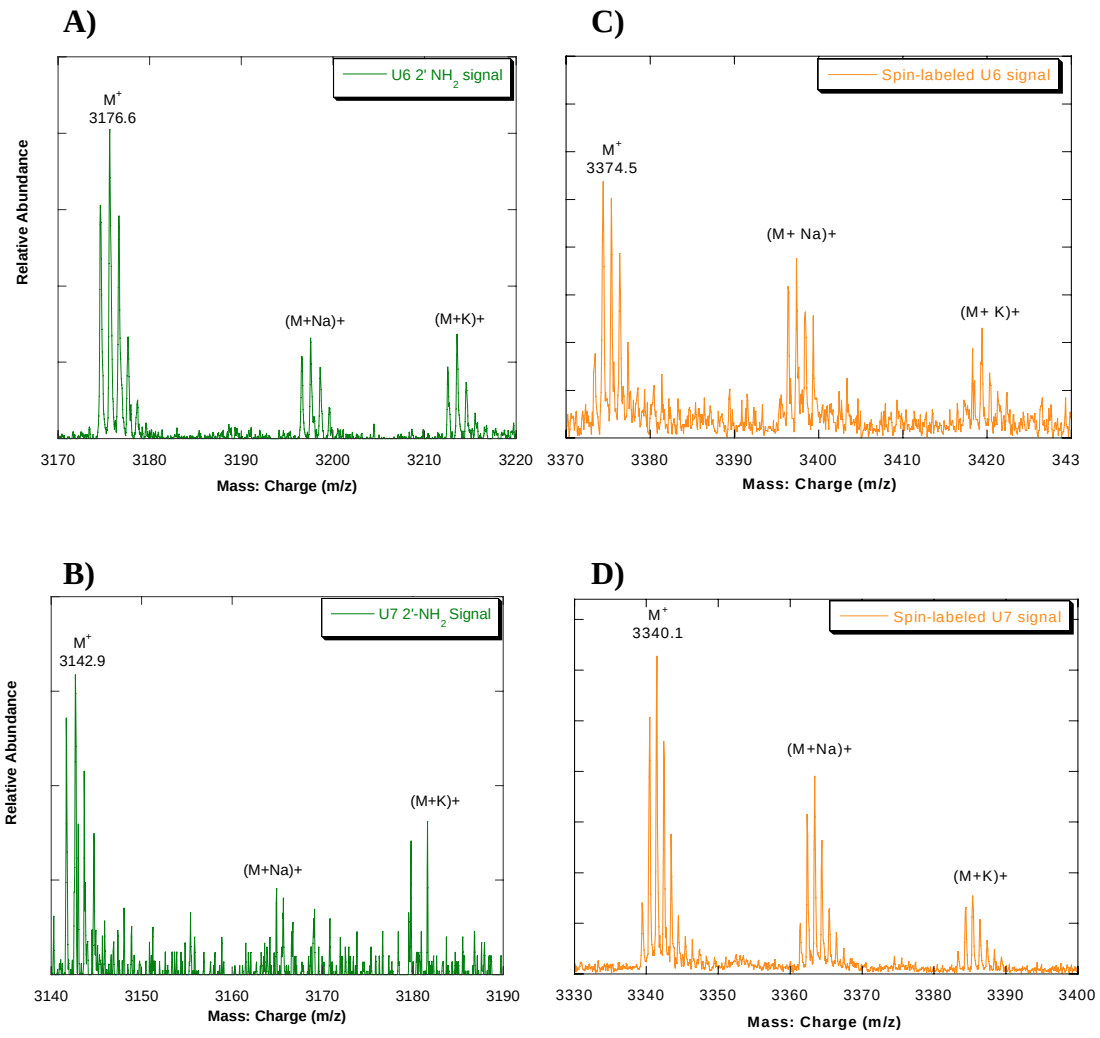

Figure 3-2: Positive ion mode MALDI-TOF-MS spectra of U6mod (A), U7mod (B), and products of spin-labeling reactions with U6 (C) and U7 (D). Diagnostic U6mod and U7mod spectra were collected which confirmed the qualitative respective spin-label attachment. Sodium and potassium adducts were observed in all spectra.

RP- HPLC purification

Despite increased spin-labeling efficiency (~ 80%) with 4-isocyano TEMPO **(2)** spin-label probe over the previously used succinimdyl-2,2,5,5-tetra-methyl-3-pyrroline-1-oxyl-carboxylate **(1)** (≤ 50 %), such spin-labeling reactions do not proceed to 100% conversion (Edwards *et al.* 2001a, Kim *et al.* 2004). Reverse-phase HPLC purification was implemented to separate spinlabeled from non-labeled RNA (Edwards et al. 2001a, Kim et al. 2004). As shown in Figure 3-3, spin-labeled RNA has higher column retention for both sequences in comparison with non-labeled strands.

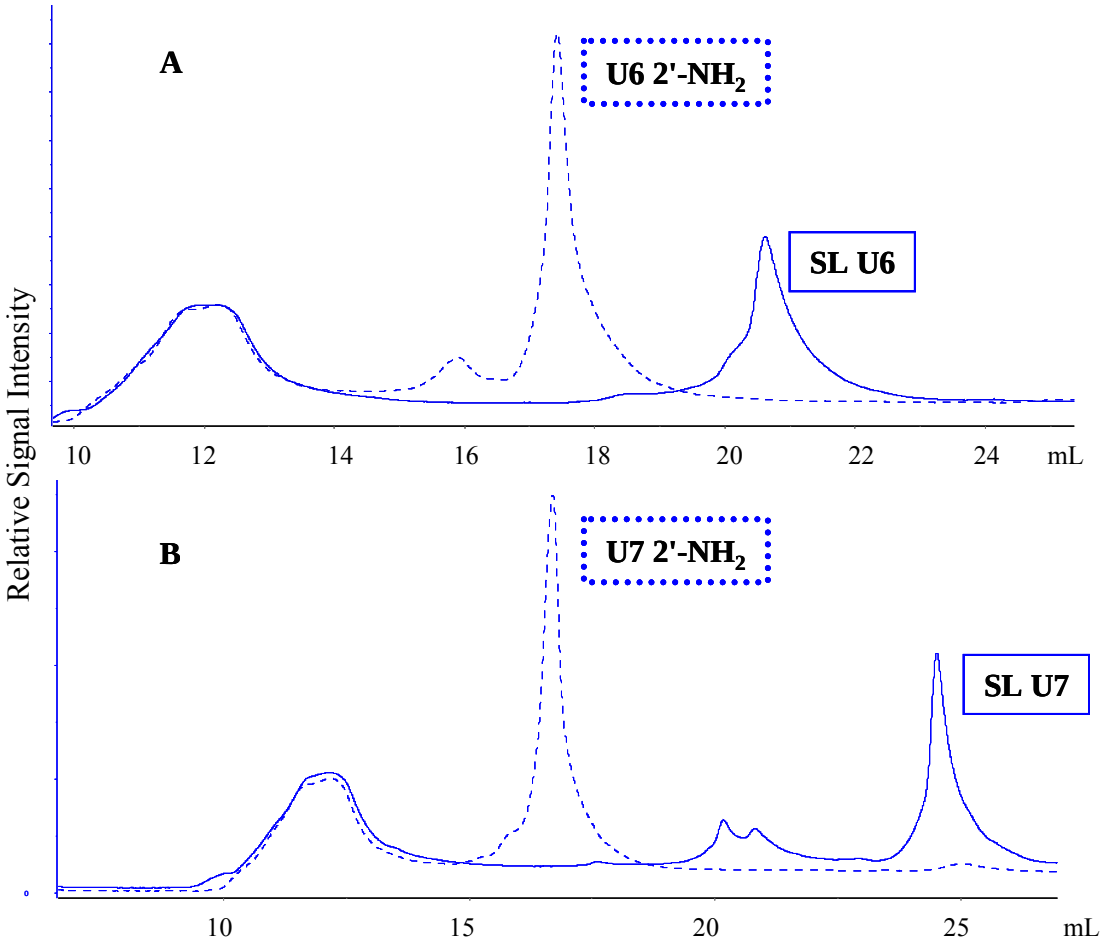

Figure 3-3: RP-HPLC spectra shows separation of non-labeled and spin-labeled RNA sequences for U6 (A) and U7 (B) monitored at 260 nm. Traces for the starting material (2'-NH_2 modified RNA) are shown in a dashed trace while spin-labeled samples are depicted with solid traces. In each case 10 nmoles of sample was loaded onto the column.

Duplex investigation *via* thermal denaturation studies

UV-Vis thermal denaturation studies investigated the thermodynamic stability of the U6-U7 duplex in wild type (WT), modified (mod) and spin-labeled (SL) samples. As shown in Table 3-3, the melting temperature (T_m) of WT U6-U7 duplex aligns well with the previous series of WT 10-mer duplexes at T_m ~55^{0}C (Kim et al. 2004). Similarly, a 2'-NH_2 modification destabilizes duplex stability by ΔT_m ~ -3 ^{0}C (Kim et al. 2004). Differences in duplex stability were observed with incorporation of spin-label probes **(1)** and **(2)**. Both spin-label probes in a 10-mer duplex greatly destabilized duplex structure, however in this research with **(2)** as the spin-label probe the duplex was further destabilized by an additional 3 ^{0}C (Kim et al. 2004).

Table 3-3: Thermal stabilities of 10-mer duplexes

Duplex Structure	Duplex Name	$T_{m,\ average}$ (^{o}C) **(1)**[b]	$T_{m,\ average}$ (^{o}C) **(2)**
U6 5' CCUAGUGUGG 3' U7 3' GGAUCACACC 5'	Wild Type	55.4	55.1
U6 5' CCUAGUGUGG 3' U7 3' GGAUCACACC 5'	2'- NH_2 modification[c]	52.3	51.8
U6 5' CCUAGUGUGG 3' U7 3' GGAUCACACC 5'	Spin-labeled	36.1	33.3

a) conditions: 2μM RNA duplex in 900 μL 5 mM TEA, pH 7.8, 100 mM NaCl
b) Taken from Kim et al. 2004
c) Duplexes contained modification/label on both U6 and U7 strands.

EPR spectroscopy

Low temperature EPR spectroscopy in conjunction with Fourier deconvolution methods were used to obtain intramolecular distance measurements in spin-label probes (Kim et al. 2004). In Figure 3-4 the summed spectra of two singly-labeled duplexes are shown in black, and the spectra of doubly-labeled duplexes are shown in red. Spectra in

(A) are spin-labeled duplexes at 183 K using **(1)** as the spin-label probe (Kim et al. 2004), while spectra in (B) implemented **(2)** as the spin-label probe and EPR data were obtained at 100 K. For both sets of spectra dipolar line broadening results in an apparent signal decrease for the doubly-labeled duplexes. Dipolar line broadening was quantitated with Fourier deconvolution methods to extract intermolecular distances. The derived U6-U7 intermolecular spin-probe average Fourier deconvolution distance ($d_{FD,\ avg}$) for **(1)** was 14.8 Å (Kim et al. 2004) and **(2)** was 16.3 Å.

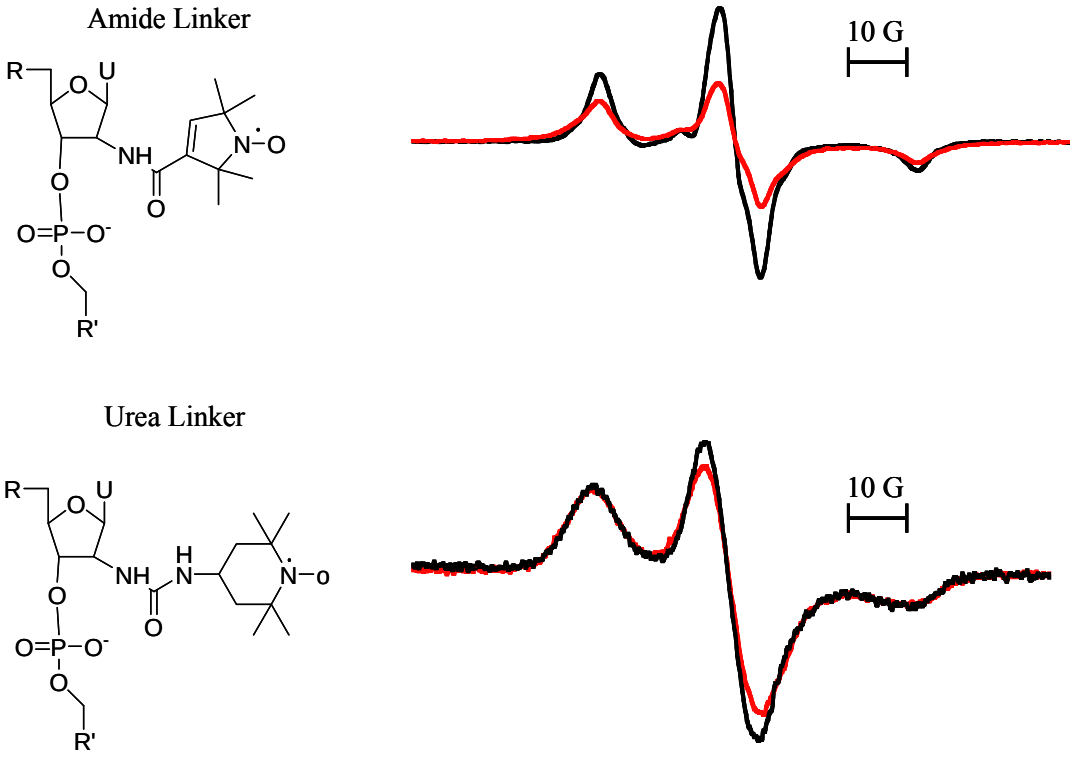

Figure 3-4: EPR spectra of the doubly-labeled 10-mer duplexes obtained at low temperature (183 K (A) and 100 K (B)) in 100 mM NaCl, 20% ethylene glycol and 5 mM TEA buffer (pH 7.8). The summed spectra of two noninteracting single-stranded duplexes are shown in black, and the spectra of interacting double spin-labeled duplexes are shown in red. Dipolar line broadening resulted in an apparent signal decrease for the doubly spin-labeled duplexes.

Molecular modeling

Molecular modeling was implemented to predict the distances between nitrogen radicals within spin-labeled duplex systems in a similar manner as Kim and coworkers (Kim et al. 2004). In these simulations the duplex region was held in a fixed energy minimized conformation while the spin-labels rotated freely. Thirty-six different starting dihedral angles were used to generate a distribution of distances. Distance distributions for the doubly spin-labeled U6-U7 duplex with **(1)** and **(2)** are shown in Figure 3-5. Further, the molecular modeling distance distribution for spin-label **(1)** and **(2)** were within the experimental range available for CW-EPR spectroscopy. Spin-label (**1**) had an average molecular modeling distance of 12.6 Å (Kim et al. 2004) while when **(2)** was modeled an average distance of 16.1 Å was calculated. The experimental $d_{FD,\ avg}$ obtained from both sets of EPR spectra are indicated with arrows. The agreement between measured and predicted distances is closer for spin-label (**2**) ($d_{MD,avg.}$ = 16.1, $d_{FD,avg.}$ = 16.3 Å) than that for (**1**) ($d_{MD,avg.}$ = 12.3, $d_{FD,avg.}$ = 14.8 Å).

Discussion

SDSL studies are useful in obtaining distance measurements in biomolecules. Spin-label attachment was promoted through 2'-NH_2 ribose modification (Edwards et al. 2001a, Edwards et al. 2001b, Kim et al. 2004) and confirmed by MALDI-MS spectrometry. The ~198 dalton shift from 2'-NH_2 modified U6 and U7 spectra was a qualitative diagnostic confirmation of 4-isocyano TEMPO spin-label probe incorporation. Further, unreactive RNA was separated from spin-labeled RNA with RP-HPLC techniques similar to those of Edwards and Kim (Edwards et al. 2001a, Kim et al. 2004). Purified spin-labeled sequences were studied as duplex systems in thermal denaturation and EPR spectroscopic studies.

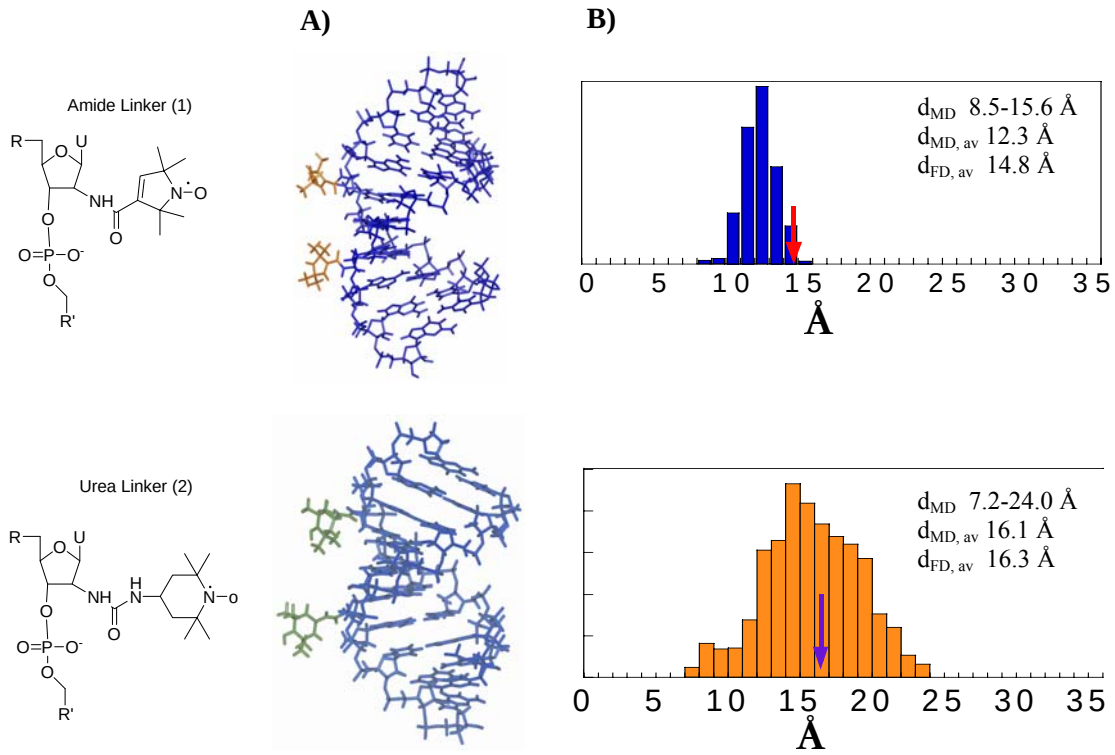

Figure 3-5: Molecular modeling of spin-labeled U6-U7 duplexes. (A) The structures of spin-labeled RNA 10-mers simulated within the Discover 3 module in *Insight II*, assuming that the 10-mers have canonical rigid A-type RNA structures and nitroxides are flexible. (B) Distributions of the interspin distances for duplexes predicted for MD calculations and the averaged interspin distances obtained from FD analysis of EPR spectra (arrow).

The U6-U7 duplex system previously investigated in this laboratory was explored in this work but with **(2)** as a spin-label probe. All controls performed aligned well with previously published data. However, in thermal denaturation studies when **(2)** was incorporated into the duplex the thermodynamic stability decreased ~3 ^{0}C. In LT EPR and molecular modeling studies it was also apparent that the differing spin-label probe influenced experimental and theoretical distance measurements. The thermal destabilization and increased distance measurements could be attributed to increased linker length and ring size in (**2**). As shown in experimental and simulation methods the intermolecular distance with (**2**) compared to (**1**) was longer and possibly more flexible which may facilitate the spin-label intercollation of the duplex as seen by the increased destabilization in thermal denaturation studies. Further, simulated and experimentally

derived intermolecular distances match well, 16.3 and 16.1 Å, respectively, when (**2**) was used as the spin-label. Attachment of the 4-isocyano TEMPO spin-label (**2**) possibly creates a more flexible urea linker compared to amide linkage in (**1**). The potential linker flexibility is reflected with better agreement between experimental and simulation data compared to a rigid linker that may not be as easily modeled. Based on these results the spin-label probe does influence stability and distance measurements.

CHAPER IV
DOUBLE SPIN-LABELING SINGLE-STRANDED RNA

Background and motivation

Distance measurements in Site-Directed Spin-Labeling (SDSL) require attachment of two spin-label probes within the system of interest. Typically, two spin-labels are incorporated by annealing single-strands, each containing a single spin-label (Edwards et al. 2001a, Kim et al. 2004, Edwards and Sigurdsson 2005, Kim et al. 2005). Figure 4-1 (**A**) depicts annealed singly spin-labeled RNA strands; the stars indicate locations of spin-label attachment. However, this methodology is limited to systems in which two oligonucleotides are annealed together. To circumvent this limitation and also to explore single-strand dynamics a new methodology was implemented, double spin-labeling. Figure 4-1 (**B**) illustrates a potential doubly spin-labeled single stranded RNA. A 10-mer model system was used to investigate the "double label" spin-labeling method. Figure 4-2 shows WT, single 2'-NH_2 modified and doubly 2'-NH_2 modified sequences where modified sites are indicated in orange.

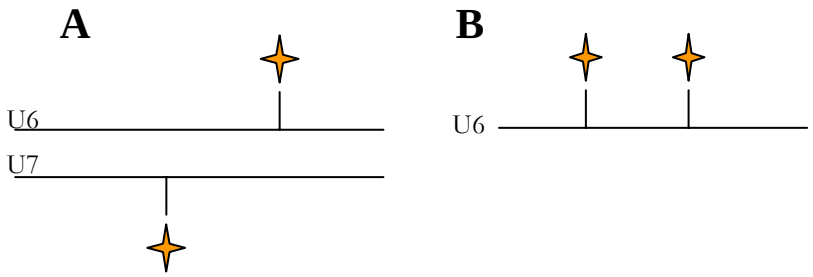

Figure 4-1: A representation of the requirement of two spin-probes for distance measurements. Single spin-probe attachment per 10-mer (**A**) compared to double spin-probe attachment (**B**).

Diagnostic mass spectrometry of spin-labeled sequences

MALDI-TOF-MS was implemented as a diagnostic tool to confirm the attachment of **(2)** to 2'-NH_2 modified positions within 10-mer RNA sequences. The 10-

mer RNA sequences studied are shown in Figure 4-2, where modifications are highlighted in orange. Sequence U6mod contains one 2'-NH_2 modification and U6 2mod has two 2'-NH_2 modifications. Initially, MALDI-TOF-MS spectra of U6mod and U62mod were obtained as shown in Figure 4-3. U6mod and U62mod molecular ions were observed at 3174 and 3175 daltons respectively, and the difference in these values correlate to the mass difference due to a modification relative to wildtype (WT) 2'-OH (3176 daltons). In addition, their corresponding sodium and potassium adducts were also observed as shown in Figure 4-3.

a) U6 WT	5'	CCUAGUGUGG	3'
b) U6 mod	5'	CCUAG**U**GUGG	3'
c) U6 2mod	5'	CC**U**AG**U**GUGG	3'

Figure 4-2: 10-mer RNA single strand sequences. 2'-NH_2 modifications are denoted in orange. U62mod was implemented for double spin-labeling purposes.

After the spin-label reaction of U62mod with 4-isocyano TEMPO spin-label, (**2**), additional MALDI-TOF-MS samples were prepared. As shown in Figure 4-3, the covalent attachment of the spin-label probe to the 10-mer sequence produced single and double spin-labeled RNA. The spin-label probe shifted the U62mod molecular ion (3174.9) to 3373 and 3569 daltons which indicates single and double spin-labeling respectively, as each spinlabel adds ~198 daltons. Sodium and potassium adducts were also seen in the singly and doubly spin-labeled samples.

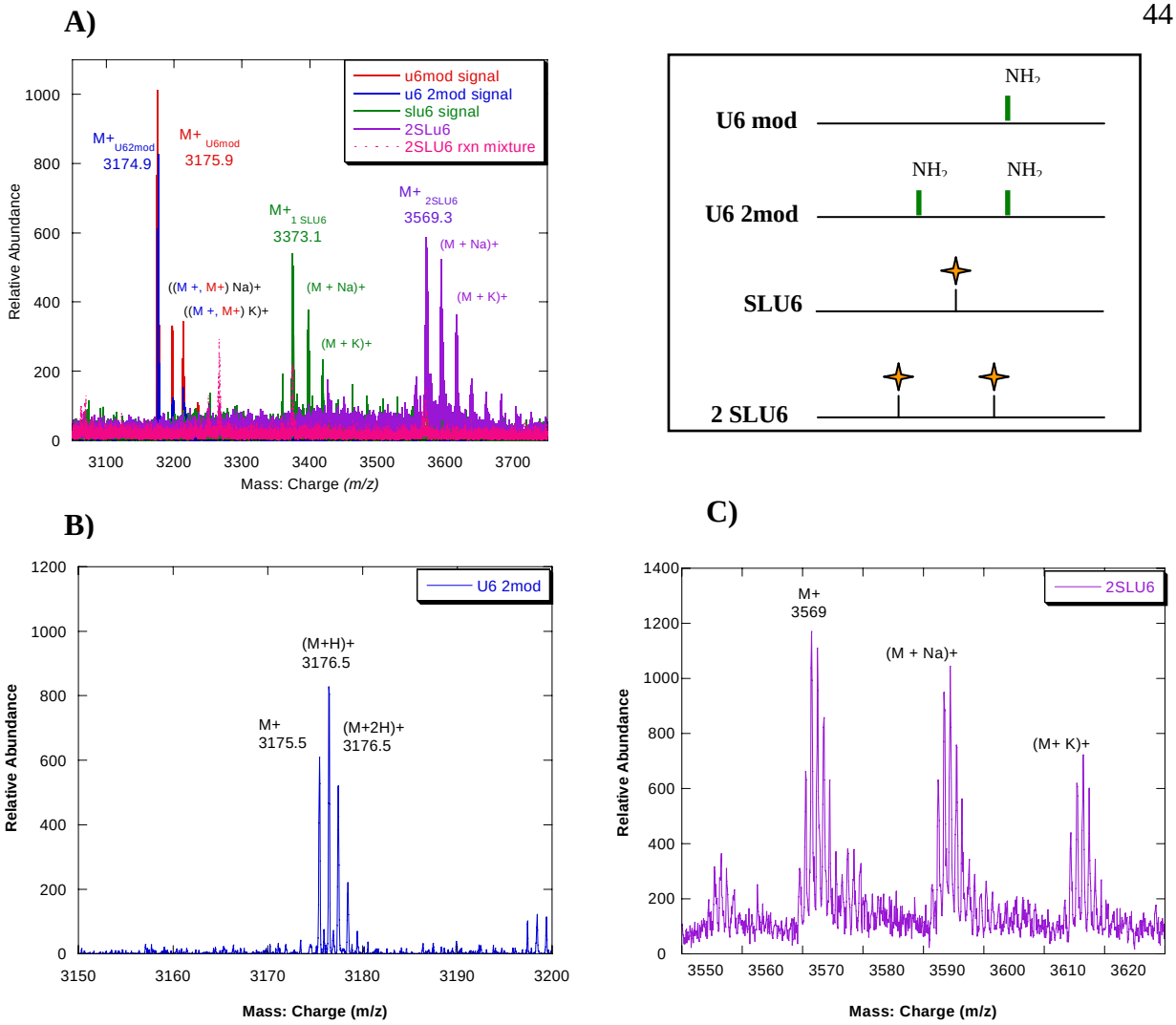

Figure 4-3: MALDI-TOF-MS spectra of 10-mer RNA sequences with 2'-NH_2 modifications and conjugated spin-labels. (**A**) is an overlay of U6mod, U62mod, singly spin-labeled U62mod and doubly spin-labeled U62mod. (**B**) is an expanded region of the U62mod region molecular ion and (**C**) is a corresponding plot for U62mod after spin-labeling. Sodium and potassium adducts were observed in all spectra.

RP-HPLC purification and peak confirmation

Spin-labeling reactions do not proceed to 100% conversion. Reverse-phase HPLC purification was implemented to separate modified, single-labeled and double-labeled RNA. As shown in Figure 4-4, double spin-labeled RNA has higher column retention compared with single spin-labeled and non-labeled strands. An injection of U62mod acted as a control and is shown in the blue dashed trace. After the spin-labeling reaction of U62mod, an aliquot of the reaction was injected and this trace is shown in solid blue. The overlay of these two samples, shown in Figure 4-4 shows three different

sets of peaks. The identities of the samples in the HPLC fractions were confirmed using MALDI-TOF-MS.

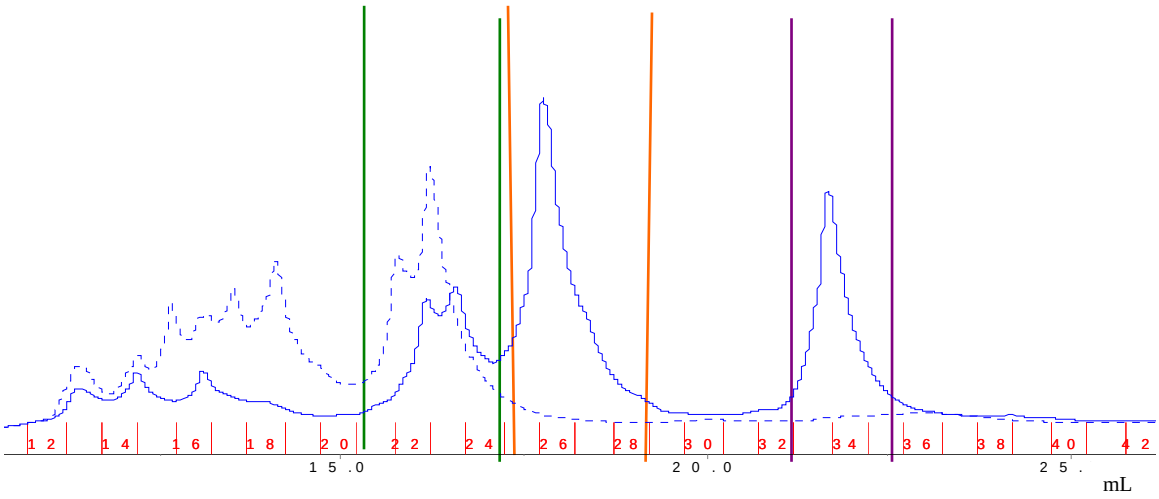

Figure 4-4: RP-HPLC overlay containing U62mod (blue dashed) and U62mod spin-labeled reaction mixture (blue solid). The total volume of the HPLC gradient is represented by the x-axis and the collected fraction (f) number is in red. MALDI-TOF-MS identified the peaks for U62mod (green f 21-24), single spin-labeled U62mod (orange f 25-28) and double spin-labeled U62mod (purple f 33-35).

MALDI-TOF-MS was implemented to identify peaks from the HPLC trace. The green region, fractions 21-24, overlaid well with the U62mod control trace and was predicted to contain U62mod. The mass spectrum of the green region, shown in Figure 4-5 (**A**), confirmed that the identity of the green region was U62mod with a molecular ion of 3174 daltons. Further, the orange region; fractions 25-28, was successfully identified as singly spin-labeled U6 with a molecular ion of 3377 daltons as shown in Figure 4-5 (**B**). The most highly retained purple region was identified as doubly spin-labeled U6 with a molecular ion at 3569 daltons as shown in Figure 4-5 (**C**).

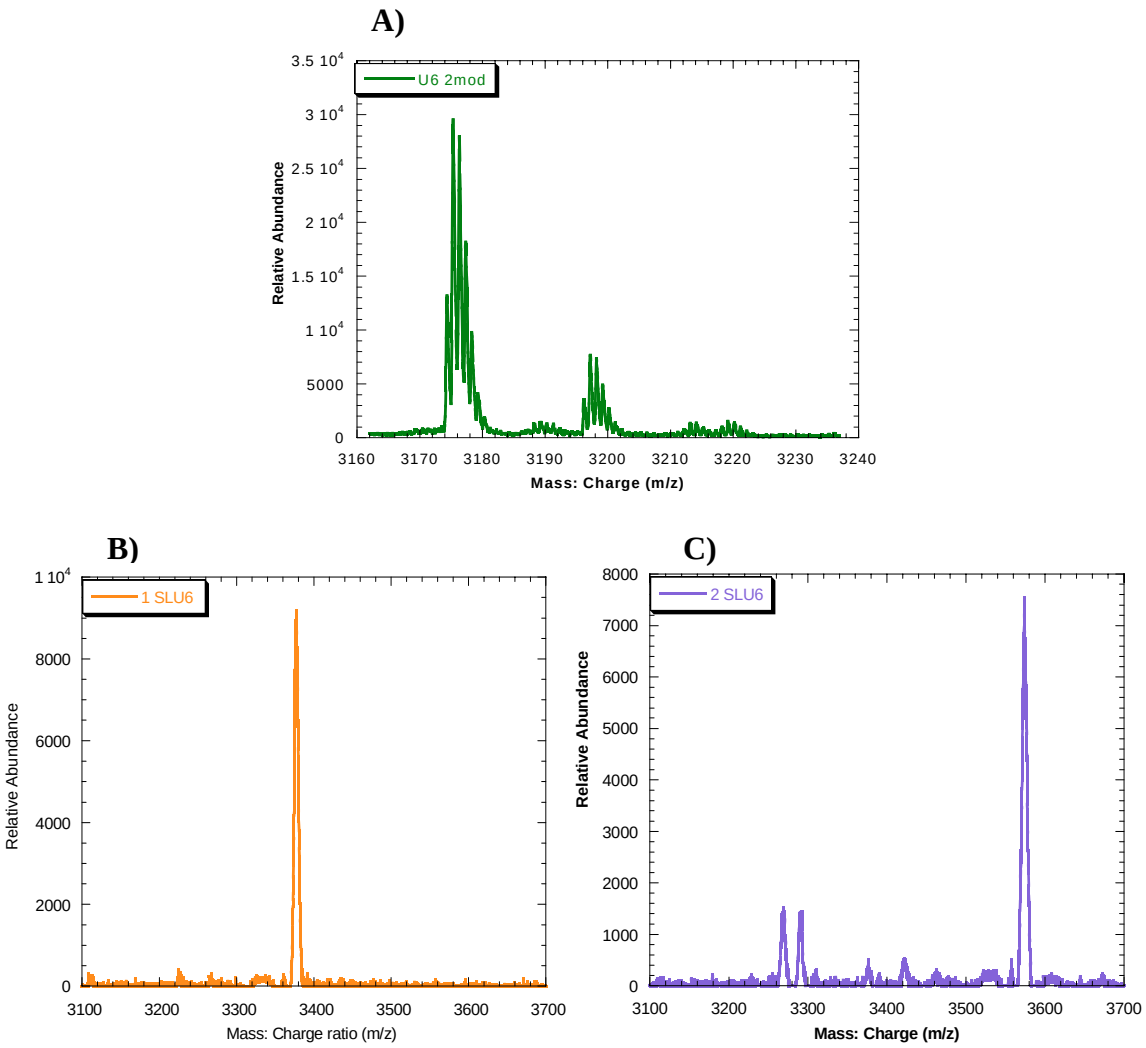

Figure 4-5: MALDI-TOF-MS confirmation of HPLC purified fractions. The green, f 21-24, contains the molecular ion for U62mod as shown in (**A**). The orange, f 25-28, (**B**) depicts the diagnostic mass spectrum of singly spin-labeled U6. The purple, f 33-35, (**C**) depicts the diagnostic mass spectrum of doubly spin-labeled U6 at 3569 daltons.

EPR spectroscopy

LT-EPR is required to investigate the doubly spin-labeled single strand. Previously, the Fourier deconvolution (FD) method was used to obtain intramolecular distance measurements of nitroxide moieties on opposing strands of the U6-U7 RNA duplex (Kim et al. 2004). In the doubly spin-labeled single strand system two spin-labels are on a single-strand. Low temperature EPR spectroscopy in conjunction with Fourier deconvolution methods were used to obtain intramolecular distance

measurements of spin-label probes. In Figure 4-6 the summed spectra of two single spin-labeled single strands are shown in black, and the spectrum of double spin-labeled single-strand is shown in orange. Spectra are spin-labeled single-strands at 100 K using **(2)** as the spin-label probe. For this set of spectra dipolar line broadening resulted in an apparent signal decrease for the double spin-labeled single-strands. Further, dipolar line broadening was measured with Fourier deconvolution methods to obtain intermolecular distances (Kim et al. 2004). The double spin-labeled single-strand had an intermolecular spin-probe average Fourier deconvolution distance ($d_{FD, avg}$) was 16.8 Å.

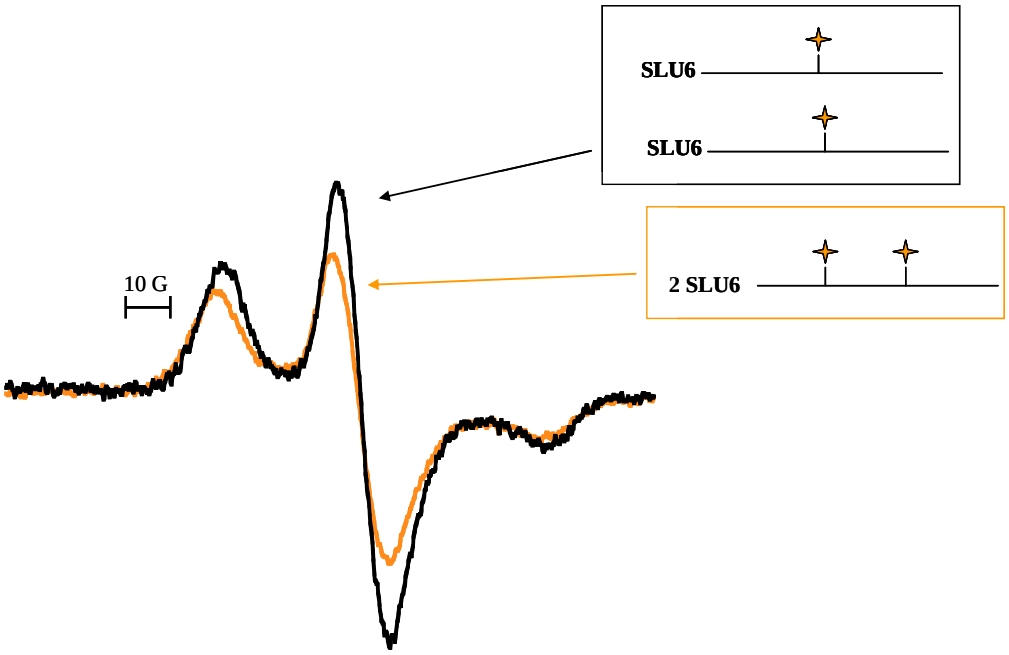

Figure 4-6: EPR spectra of double spin-labeled RNA oligonucleotides. LT- EPR spectra of 29 mM doubly-labeled 10-mer single strand at 100 K in 100 mM NaCl, 20% ethylene glycol and 5 mM TEA buffer (pH 7.8). The summed spectra of two singly-labeled single-strands are shown in black, and the spectra of doubly-labeled single-strand shown in orange.

The double spin-labeled single-strand was also explored within a duplex (2SLU6-U7). LT-EPR with FD methods were used to obtain intermolecular distance measurements between the spin-label probes. In Figure 4-7 the summed spectra of two

single spin-labeled U6-U7 duplex strands are shown in black and the spectra of a double spin-labeled single-strand within a duplex (2SLU6-U7) is shown in red. Dipolar line broadening was observed and measured with FD methods to obtain an average intermolecular distance value of 19.8 Å.

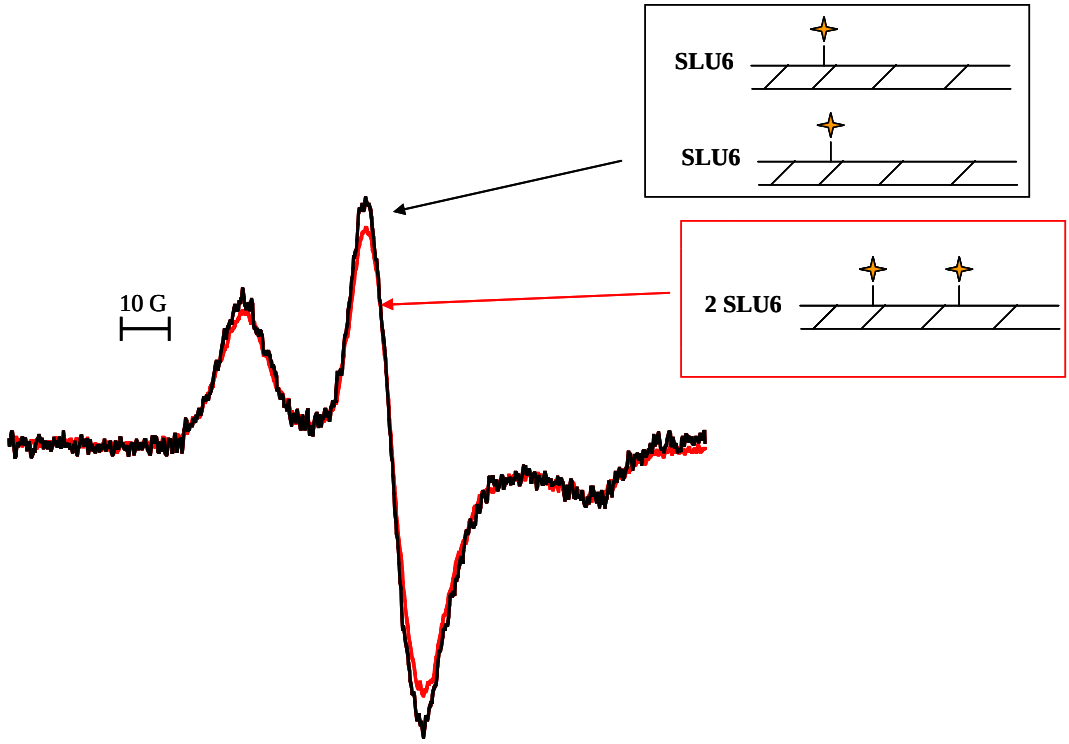

Figure 4-7: EPR spectra of double spin-labeled single-stranded RNA in a 2SLU6-U7 duplex. LT- EPR spectra of a 29 mM double spin-labeled 10-mer single strand in duplex was measured at 100 K in 100 mM NaCl, 20% ethylene glycol and 5 mM TEA buffer (pH 7.8). The summed spectra of two singly-labeled duplex strands are shown in black, and the spectra of doubly-labeled single-strand within duplex is shown in red.

Molecular modeling

Previous molecular modeling implemented the Discover 3 module of Unix-based Insight II for molecular mechanics (MM) and molecular dynamics (MD) to calculate intermolecular distances. In that modeling design the U6-U7 duplex region was "fixed" and the only the nitroxide spin-labels rotated freely. Also, the RNA duplex was in a constant medium with a set dielectric constant. As a first attempt, a similar modeling

design was used to project the intermolecular distances of the nitroxide probes in a single- stranded system.

The U6-U7 duplex was constructed with two spin-probes placed on designated positions on the U6 strand. The duplex region was held in a rigid position and the spin-labels were allowed to rotate freely in a constant dielectric medium. The results of the molecular modeling are displayed in Figure 4-8. Distances were calculated from a series of x-y-z coordinates and these values range from 9.6- 26.1 Å. As shown in Figure 4-8, the average intermolecular distance between the nitroxide probes was 18.9 Å with MD simulations compared to an experimental value of 16.8 Å obtained with FD methods (orange arrow).

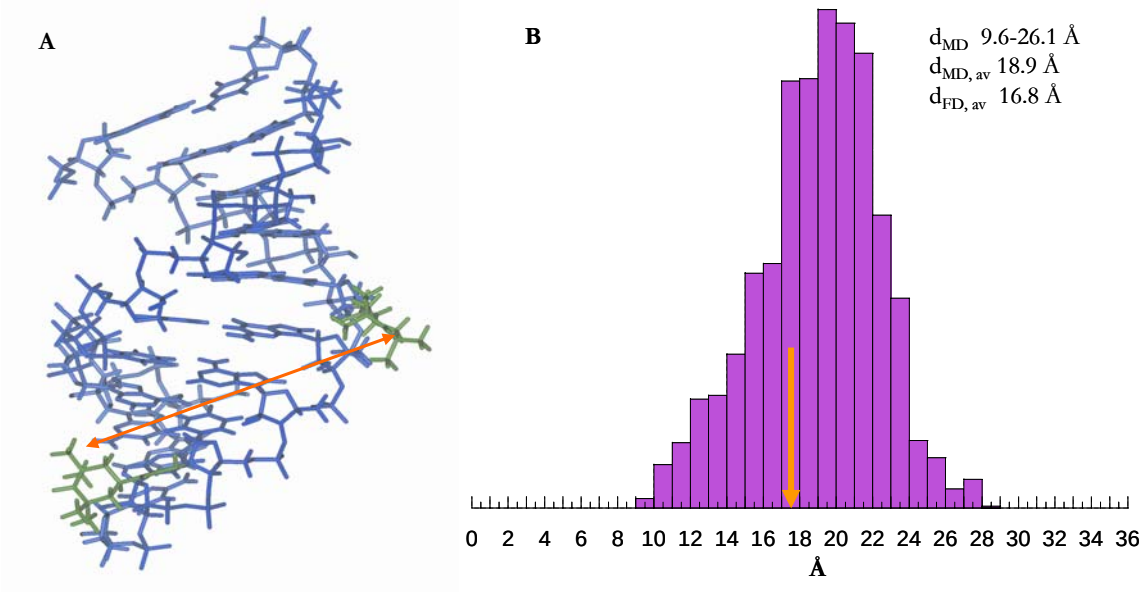

Figure 4-8: Prediction of interspin distances for double spin-labeled single strand using molecular modeling simulations. A double spin-labeled U6 in duplex (2SLU6- U7) was energy minimized (**A**) and this structure used as a basis in MS calculations. (**B**) The distribution and the average interspin distances MD_{avg} are plotted with the average distance obtained by experimental FD analysis of EPR spectra (orange arrow).

Discussion

SDSL studies are helpful in determining distance measurements within biological systems. Two spin-labels are required for distance determinations. In previous RNA SDSL studies a single spin-label probe was attached to a single-strand and the two strands were annealed to obtain distance measurements (Kim et al. 2005, Kim et al. 2004). However, in larger biological systems this single spin-labeling methodology is challenged as there may not be two convenient pieces for spin-labeling. There is a risk in splitting a single-stranded sequence as the strands may not anneal in the correct structure and the biological activity could be disrupted. These motivating factors prompted the study of a double spin-labeled single-strand. A 10-mer RNA model system was implemented to explore the possibility of double spin-labeling.

A spin-labeling reaction with 4-isocyano TEMPO (**2**) on the U62mod sequence achieved covalent attachment of the spin-probe. Singly and doubly spin-labeled U6 was generated from the reaction and confirmed *via* MALDI-TOF-MS. Further, doubly spin-labeled U6 was RP-HPLC purified from incompletely labeled RNA sequences. The efficiency of single to double spin-labeling in U62mod was a 1:1 ratio regardless of spin-labeling conditions. In an initial optimization reaction study increased volume of spin-label (10X) and reaction time (from 2- 18 hours) showed no difference in spin-labeling efficiency.

Intermolecular distances of the spin-probes were calculated with experimental LT-EPR spectroscopy in conjunction with computational simulations. In this study LT-EPR with FD methods calculated an intermolecular distance of 16.8 Å for double spin-labeled single-stranded RNA compared to 19.8 Å for a double spin-labeled single-strand within a duplex. The difference (16.8 vs. 18.9 Å) between experimental double spin-labeled single-stranded RNA and double spin-labeled single-strand within a duplex in the MD calculations obtained intermolecular distance measurements were greater than the single spin-labeled single-stranded U6-U7 duplex (d_{MD} = 16.1, d_{FD} = 16.3 Å). One possible reason for the increased error could be that these initial conditions for molecular modeling and molecular dynamic calculations may not be rigorous enough for distance measurements. In comparison, the double spin-labeled single strand within a duplex (2SLU6-U7) had a better agreement between experimental and simulated methods with

d_{FD}= 19.8 Å and d_{MD}= 18.9 Å respectively. The double spin-labeled single strand had a smaller distance (d_{FD} = 16.8 Å) which could suggest that the two spin-label probes are in a more rigid conformation within a duplex (d_{MD} = 19.8 Å). These results may be an indication of single-strand flexibility in RNA.

CHAPTER V
CONCLUSIONS

Conclusions

This thesis focuses on SDSL studies within 10-mer RNA model systems. A 10-mer RNA duplex was used to probe the role of the spin-label in obtaining distance measurements. In previously published work succinimdyl-2,2,5,5-tetramethyl-3-pyrroline-1-oxyl-carboxylate (**1**) was used as the spin-label probe in the U6-U7 RNA duplex (Kim et al. 2004), resulting in an 2'-amide linker to a 5-membered nitroxide ring. While this spin-labeling method is convenient because it uses a commercially available substrate with a succinimdyl leaving group, the conjugation efficiency was $\sim \leq 50\%$. In this research an isocyanate derivative of tetramethylpiperidyl-N-oxy (TEMPO) **(2)** was implemented within the U6-U7 duplex giving a 2'-urea linked 6-membered nitroxide ring (Edwards et al. 2001a) and the influence of this probe was studied. Spin-label (**2**) requires a one-pot synthesis strategy with commercially available 4-amino TEMPO and the resulting 4-isocyano TEMPO spin-label produced an RNA spin-labeling efficiency > 90%.

MALDI-TOF-MS confirmed covalent attachment of (**2**) in the U6 and U7 sequences (Figure 3-2). Signature RP-HPLC traces for spin-labeled and non-labeled RNA were found, and spin-labeled RNA was successfully purified (Figure 3-3). As shown in Table 3-3, thermal denaturation studies aligned well with WT and 2'-NH_2 modified sequences previously studied (Kim et al. 2004). In a spin-labeled duplex (**2**) decreased the thermal stability by an additional 3 ^{0}C compared to (**1**) (Kim et al. 2004). The intermolecular distance between two nitroxide moieties in the U6-U7 RNA oligonucleotide was determined with experimental and theoretical methods (Figure 3-5). LT-EPR spectroscopy in conjunction with FD convolution methods calculated an intermolecular distance of 16.3 Å while molecular modeling (MM) simulations within the Discover 3 module within *Insight II* provided a range of distances (7.2 – 24 Å) with an average value of 16.1 Å. In both methods when (**2**) was the spin-label probe the intermolecular distance calculated was longer than those for (**1**) (Kim et al. 2004). The agreement between experimental and simulations using (**2**) was better (16.3 vs. 16 Å) in comparison with results using (**1**) (14.8 vs. 12.3 Å).

Double spin-labeling of a single RNA strand would be advantageous in cases where the system was not amenable to annealing of two separate labeled strands, as has been previously done (Edwards et al. 2001a, Kim et al. 2004, Kim et al. 2004). Double spin-labeling of a 10-mer RNA single strand containing two 2'-NH_2 modifications was confirmed *via* MALDI-TOF-MS (Figure 4-3). The yield of double spin-labeled U6 was ~ 40 % and the yield of single spin-labeled U6 was ~ 40 %.

Initial LT-EPR spectroscopy and molecular modeling studies were also performed to calculate intermolecular distance of nitroxide moieties in an RNA oligonucleotide when in a double spin-labeled single-strand. Experimental values for the distance between nitroxide moieties in a double spin-labeled single-strand (d_{FD} = 16.8 Å) and within a duplex (2SLU6-U7) (d_{FD} = 19.8 Å) were measured. The experimental distance measured for the double spin-labeled single-strand within a duplex aligned well with the simulated distance (d_{FD} = 19.8 Å, d_{MD} = 18.9 Å). These data suggest a method to monitor possible single-strand flexibility.

Future directions

Double spin-labeling 10-mer RNA model systems

The ability to attach two spin-labels in a single 10-mer RNA strand with reasonable yields has been established. Further exploration within a simple 10-mer model system could be performed in order to optimize yield. Initial studies monitoring the influence of spin-label concentration, temperature and reaction time may provide insights for optimizing double spin-labeled single RNA strands. Does the distance between the 2'- NH_2 modifications for covalent attachment of the spin-label probes influence spin-labeling efficiency? After establishing an optimized yield procedure of U62mod 2'- NH_2 modifications could be placed at the various positions within a 10-mer RNA to investigate labeling efficiency based on sequence position. In this research one nucleotide separated the two 2'- NH_2 modifications. The amount of space between spin-labels in spin-labeled U6 2mod may have created steric bulk and inhibited spin-labeling efficiency as observed by the appearance of single spin-labeled U6 2mod. If the spin-label probes are separated by a greater number of nucleotides this may increase the spin-labeling efficiency as the steric bulk interaction could be reduced.

MALDI-TOF-MS might be used to determine whether there is a preference for site labeling in the U62mod RNA strand. Single spin-labeled U62mod could be produced in two conformations as shown in Figure 5-1 (b and c). MALDI-TOF-MS of single spin-labeled U62mod has a single molecular ion regardless of confirmation. MALDI-TOF-MS-MS could be used to explore if a site preference does exist. An MS-MS method may provide unique diagnostic molecular ions and although MS is not a qualitative technique the relative abundance could be an indication of preferred confirmation.

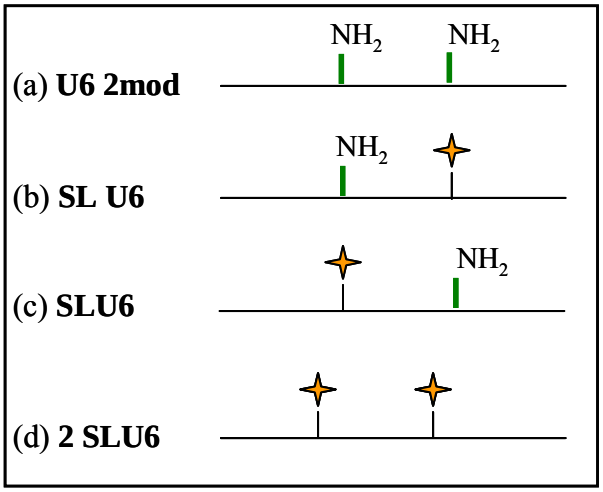

Figure 5-1: A spin-labeling reaction with (a) a 10-mer RNA single-strand with spin-label (**2**) produces single spin-labeled (b and c) and double spin-labeled (d) RNA. Further MALDI-TOF-MS experiments might be able to distinguish between options (b) and (c).

As previously mentioned, the phosphate backbone is a key structural component that contributes to prevalent electrostatic forces that influence RNA folding. The electrostatic repulsion between the negatively charged phosphate moieties is minimized by the addition of counter-ions such as mono(M^{+})- or divalent (M^{+2}) metal ions which are often required for RNA folding. Under varying M^{+} and M^{+2} metal ions in solution this 10-mer RNA model may provide insights about single-strand environment that can be directly explored with LT-EPR spectroscopy. LT-EPR in conjunction with FD methods could monitor any changes in distance measurements due to the presence of metal cations. If the addition of M^{+} and M^{+2} perturbs the intermolecular distance this would reflect

single-strand flexibility. Performing similar metal ion solution studies on double spin-labeled 10-mer RNA on varied two 2'-NH_2 modified positions would provide a cohesive picture about single-strand RNA flexibility.

Folding pathway of larger RNA systems

The P4-P6 structural domain is a stable subdomain of the Group I intron (Doudna and Cech 1995). The secondary structure for the 160 nucleotide P4-P6 domain is shown in Figure 5-2 (Doudna and Cech 1995). Further, the P4-P6 domain folding studies of the Group I intron from *Tetrahymena thermophilia* have shown that the P4-P6 domain folds first and independently of the rest of the intron (Latham and Cech 1989, Celander and Cech 1991, Murphy and Cech 1993, Laggerbauer et al. 1994, Wang et al. 1994, Woodson 2002). The isolated P4-P6 domain adopts the same secondary structure and tertiary fold as seen when included with the rest of the intron (Laggerbauer et al. 1994, Wang et al. 1994, Cech and Doundna 1996).

A folding pathway for the P5abc subdomain of the P4-P6 domain of the Group I Intron from *Tetrahymena thermophilia* has been proposed using EPR microwave power saturation studies and other spectroscopic techniques (Burns 2004). Employing SDSL and other techniques may confirm this proposed folding pathway. SDSL studies would be specifically interesting because an RNA system of this size has not been investigated using this method. Spin-probes can be used to monitor local motions and obtain distance measurements which would provide insight into folding of this RNA. In a published x-ray crystal structure, the A-rich bulge of P5abc contains six Mg^{2+} ions, and this metal ion core is thought to be responsible for the folding of the subdomain and the P4-P6 domain (Cate et al. 1996, Cate et al. 1997). The secondary structure rearrangement of truncated P5abc subdomain in the presence of Mg^{+2} is shown in Figure 5-3 (Wu and Tinoco 1998). Nucleotides that change their base pairing with metal addition are shown in red. If spin-labels are placed near or within the A-rich bulge it may be possible to monitor the folding pathway of the P5abc subdomain.

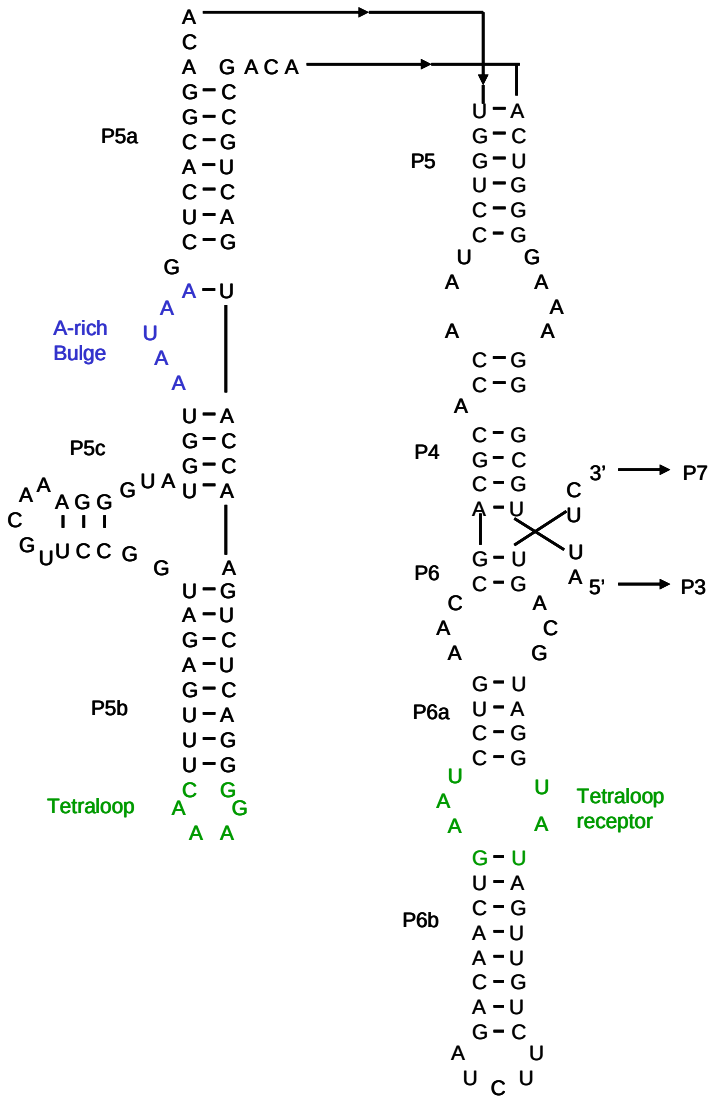

Figure 5-2: Secondary structure of the P4-P6 domain (Burns 2004).

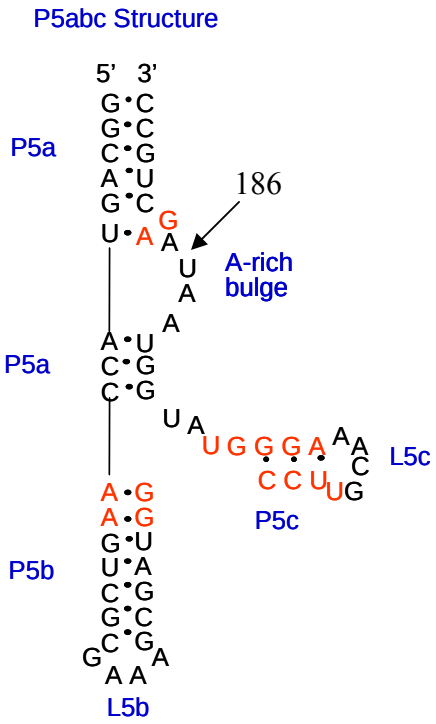

Figure 5-3: Secondary structure rearrangement of truncated P5abc in the presence of Mg^{2+} (Wu and Tinoco 1998). Nucleotides that change their base pairing with metal addition are shown in red.

Choosing sites for 2'-NH_2 modifications required for spin-label attachment will require careful consideration. There are two main concerns with SDSL studies within the P5abc system which include, RNA folding perturbation caused by SDSL and distance limitations of the X-band CW EPR for spin-labeled sites. Previous studies of the P5abc implemented a negative control by mutating position 186 within the metal ion core of the A-rich bulge from an adenine to uridine which inhibited P5abc folding (Burns 2004). Position 186 with the uridine mutation would be beneficial for amino modification and subsequent spin-label attachment therefore it could also be used as a negative folding control. For a positive folding control the sites for 2'-NH_2 modification and subsequent spin-labeling should be "naturally" occurring U and C, as not to cause additional folding disruptions as was seen in the A186U mutant. Although natural U and C could reduce base substitution affects observed with A186U, the attachment of the spin-label probe may disrupt folding. To achieve distance measurements within P5abc spin-label pairs between P5a, P5b and P5c should be chosen. X-band CW-EPR spectroscopy is limited to

~25 Å, and greater distances may require pulsed EPR techniques which measure up to ~80 Å. (Bowman et al. 2004, Schiemann et al. 2004, Kim et al. 2005).

Distance measurements can be obtained from LT CW-EPR SDSL methodologies (Kim et al. 2004). Divalent metal ions are required for the P5abc subdomain to fold. Monitoring the intermolecular distance of spin-label pairs as a function of metal ion concentration with LT CW-EPR has potential towards a folding pathway because the distance between the spin-label pairs should decrease as a function of metal ion concentration as it is thought that this is the driving force for folding. In previously published work Mn^{+2} was used as a spectroscopic probe in EPR microwave power saturation studies to determine the number of Mn^{2+} equivalents required for the metal ion core formation which is thought to be responsible for the folding of the P5abc subdomain (Burns 2004). However manganese and nitroxide radicals have g-values that overlap in X-band frequencies and separation of these overlapping signals may not be possible. Implementing Mg^{+2} is a good substitution based on previous studies that indicated similar crystal structures with Mn^{+2} and Mg^{+2} ions (Cate et al. 1996, Cate et al. 1997). Therefore magnesium as the divalent metal source could be used in the SDSL and EPR microwave power saturation studies when monitoring EPR spectra as a function of added divalent metal equivalents.

Folding assays should also be used to assess P5abc folding. Upon spin-labeling two potential techniques could be used to study the folding pathway of the spin-labeled P5abc: thermal denaturation and hydroxyl radical footprinting. Thermal denaturation profiles for P5abc, its components, and the P4-P6 domain have been well-established in previous work (Burns 2004). Based upon previous studies spin-labeling does destabilize secondary structure, however large changes in the thermal denaturation profiles would suggest that SDSL perturbs the structure (Kim et al. 2004).

Hydroxyl radical footprinting is used to monitor folding in biological systems (Woodson 2002, Tullius and Greenbaum 2005). This method requires generation of a hydroxyl radical, typically achieved through a Fenton reaction of iron (II) EDTA with hydrogen peroxide (Tullius and Greenbaum 2005). The generated radical cleaves exposed bonds from the ribose sugar and cleavage bands denote regions that are not protected from the hydroxyl radical. The exposure implies that the residues are not

incorporated within the folded metal ion core. Spin-labeling sites within these regions of protection might disrupt folding. A folding assay with this method could compare the footprinting of WT and spin-labeled P5abc as a function of metal ion concentration (Burns 2004). Both Mg^{2+} and Mn^{2+} should be used to observe any differences due to metal characteristics.

It would also be interesting to explore the complete P4-P6 subdomain of the Group I Intron with SDSL studies. As previously mentioned, attachment of (**2**) for SDSL studies of RNA requires 2'-NH_2 modifications. The entire P4-P6 domain with sequence modifications is not commercially available. Based upon the sequence position for 2'-NH_2 site modifications, two pieces could be purchased and spin-labeled and joined through a splint-mediated ligation. RNA T4 ligase could be implemented to promote phosphodiester bond linkage and this process is depicted in Figure 5-4 (Walker et al. 1975). Spin-labeling reactions should be performed before ligation as spin-labeling a longer strand may be more difficult. SDSL, EPR power microwave studies and hydroxyl radical footprinting studies should be performed in an analogous manner as that outlined for the P5abc subdomain.

Figure 5-4: Splint-mediated ligation implementing RNA T4 ligase.

REFERENCES

Altenbach, C., Marti, T., Khorana, H. G., Hubbell, W. L. 1990. Transmembrane protein structure: spin labeling of bacteriorhodopsin mutants. *Science* **248:** 1088-1092.

Bassi, G. S., Mollegaard, N. E., Murchie, A. I, and Lilley, D. M. 1999. RNA folding and misfolding of the hammerhead ribozyme. *Biochemistry* **38:** 3345-3354.

Bennati, M. and Prisner, T.F. 2005. New developments in high field electron paramagnetic resonance with applications in structural biology. *Rep. Prog. Phys.* **68:** 411-448.

Bowman, M. K., Maryasov, A. G., Kim, N.-K., DeRose, V. J. 2004. Visualization of distance distribution from pulsed double electron-electron resonance data. *Applied Magn. Res.* **26:** 23-29.

Burns, S.N. 2004. Investigation of an unusual metal-RNA cluster in the P5abc subdomain of the group I intron. Ph.D. dissertation, Texas A&M University, College Station, TX.

Cate, J. H., Gooding, A. R., Podell, E., Zhou, K., Golden, B. L., Kundrot, C. E., Cech, T. R., and Doudna, J. A. 1996. Crystal structure of a group I ribozyme domain: principles of RNA packing. *Science* **273:** 1678-1685.

Cate, J. H., Hanna, R. L., and Doudna, J. A. 1997. A magnesium ion core at the heart of a ribozyme domain. *Nat Struct Biol* **4:** 553-558.

Cech, T. R. 1990. Self-splicing of group I introns. *Annu Rev Biochem* **59:** 543-568.

Cech, T. R., and Doudna, J. A. 1996. Crystal structure of a group I ribozyme domain: principles of RNA packing. *Science* **273:** 1678-1685.

Celander, D. W., and Cech, T. R. 1991. Visualizing the higher order folding of a catalytic RNA molecule. *Science* **251:** 401-407.

DeRose, V. J. 2002. Two decades of RNA catalysis. *Chem. Biol.* **9:** 961-969.

DeRose, V. J. 2003. Metal ion binding to catalytic RNA molecules. *Curr. Opin. Struct. Biol.* **13:** 317-324.

Doherty, E. A., and Doudna, J. A. 2000. Ribozyme structures and mechanisms. *Annu Rev. Biochem.* **69:** 597-615.

Doudna, J. A., and Cech, T. R. 1995. Self-assembly of a group I intron active site from its component tertiary structural domains. *RNA* **1:** 36-45.

Doudna, J.A. and Cech, T.R. 2002. The chemical repertoire of natural ribozymes. *Nature* **418:** 222-228.

Draper, D.E. 2004. A guide to ions and RNA structure. *RNA* **10**: 335-343.

Dugas, H. 1977. Spin-labeled nucleic acids. *Acc. Chem. Res.* **10:** 47-54.

Edwards, T.E., Okonogi, T.M., Robinson, B.H. and Sigurdsson, S.Th. 2001a. Site-specific incorporation of nitroxide spin-labels into internal sites of the TAR RNA; structure-dependent dynamics of RNA by EPR spectroscopy *J. Am. Chem. Soc.* **123:** 1527-1528.

Edwards, T.E., Robinson, B.H. and Sigurdsson, S.Th. 2001b Identification of amino acids that promote specific and rigid TAR RNA-tat protein complex formation. *Chem. Biol.* **12:** 329-337.

Edwards, T.E. and Sigurdsson, S.Th. 2005. EPR spectroscopic analysis of U7 hammerhead ribozyme dynamics during metal ion induced folding. *Biochemistry* **44:** 12870-12878.

Fedor, M.J. and Williamson, J.R. 2005. The catalytic diversity of RNAs. *Nature Rev. Mol.Cell Biol.* **6:** 399-412.

Guerrier-Takada, C., Gardiner, K., Marsh, T., Pace, N. and Altman, S. 1983. The RNA moiety of ribonuclease P is the catalytic subunit of the enzyme. *Cell* **35:** 849-857.

Hoffman, B.M., Schofield, P., Rich, A. 1969. Spin-labeled transfer RNA. *Proc. Natl. Acad. Sci.* **62:** 1195-1202.

Hubbell, W.L., Cafiso, D.S., Altenbach, C. 2000. Monitoring conformational changes with site directed spin labeling. *Nature* **7:** 735-739.

Hubbell, W.L., Gross, A., Langen, R., Lietzow, M.A. 1998. Recent advances in site -directed spin-labeling of proteins. *Curr. Opin. Struct. Biol*.**4:** 649-656.

Hustedt, E.J., and Beth, A.H. 1999. Nitroxide spin-spin interactions: applications to protein structure and dynamics. *Annu. Rev. Biophys. Biomol. Struct*. **28:** 129-153.

Jeschke, G. 2003. Electron paramagnetic resonance: recent developements and trends. *Curr. Opin. Solid State & Mat. Sci.* **7:** 181-188.

Kim, N.-K., Murali, A., DeRose, V.J. 2004. A distance ruler for RNA using EPR and site-directed-spin-labeling. *Chem. Biol.* **11**: 939-948.

Kim, N.K., Murali, A., DeRose, V.J. 2005. Seperate metal requirements for loop interactions and catalysis in the extended hammerhead ribozyme. *J. Am. Chem. Soc.* **127:** 14134-14135.

Kruger, K., Grabowski, P. J., Zaug, A. J., Sands, J., Gottschling, D. E., and Cech, T. R. 1982. Self-splicing RNA: autoexcision and autocyclization of the ribosomal RNA intervening sequence of *Tetrahymena*. *Cell* **31:** 147-157.

Laggerbauer, B., Murphy, F. L., and Cech, T. R. 1994. Two major tertiary folding transitions of the *Tetrahymena* catalytic RNA. *EMBO J* **13:** 2669-2676.

Latham, J. A., and Cech, T. R. 1989. Defining the inside and outside of a catalytic RNA molecule. *Science* **245:** 276-282.

Lilley, D.M. 2003. The origins of RNA catalysis in ribozymes. *Trends in Biochemical Sciences* **28:** 495- 501.

Lohse, P.A. and Szostak, J.W. 1996. Ribozyme-catalyzed amino-acid transfer reactions. *Nature* **381:** 442-444.

Macosko, J.C., Pio, M.S., Tinoco, I. Jr. and Shin, Y.K. 1999. A novel 5' displacement spin-labeling technique for electron paramagnetic resonance spectroscopy of RNA. *RNA* **5:** 1158-1166.

Miller, J.N. 2005. Fluorescence energy transfer methods in bioanalysis. *Analyst*. **130:** 265-270.

Misra, V.K. and Draper, D.E. 1998. On the role of magnesium ions in RNA stability. *Biopolymers* **48:** 113-135.

Murphy, F. L., and Cech, T. R. 1993. An independently folding domain of RNA tertiary structure within the *Tetrahymena* ribozyme. *Biochemistry* **32:** 5291-5300.

Pham, J.W., Radhakrishnan, I. and Sontheimer, E.J. 2004. Thermodynamic and structural characterization of 2'-nitrogen-modified RNA duplexes. *Nucleic Acids Res.* **32:** 3446-3455.

Pyle, A.M. 2002. Metal ions in the structure and function of RNA. *J. Biol. Inorg. Chem.* **7:** 679-690.

Qin, P.Z., Hideg, K., Feigon, J. and Hubbell, W.L. 2003. Monitoring RNA base structure and dynamics using site-directed spin labeling. *Biochemistry* **42:** 6772-6783.

Qin, P.Z.; Dieckmann, T. 2004. Application of NMR and EPR methods to the study of RNA. *Curr. Opin. Struct. Biol.* **14:** 350-359.

Rabenstein, M. and Shin, Y.-K. 1995. Determination of the distance between two spin labels attached to a macromolecule. *Proc. Natl. Acad. Sci.* **92:** 8239-8243.

Samples. C.R., Howard, T., Raushel, F.M. and DeRose, V.J. 2005. Protonation of the binuclear metal center within the active site of phosphotriesterase. *Biochemistry* **44:** 11795-11810.

Schiemann, O., Weber, A., Edwards, T.E., Prisner, T.F. and Sigurdsson, S.T. 2003. Nanometer distance measurements on RNA using PELDOR. *J. Am. Chem. Soc.* **125:** 3434-3435.

Schiemann, O., Piton, N., Mu, Y., Stock, G., Engels, J.W. and Prisner,T.F. 2004. A PELDOR-based nanometer distance ruler for oligonucleotides. *J. Am. Chem. Soc.* **126:** 722-729.

Schroeder, R., Barta, A. and Semrad, K. 2004. Strategies for RNA folding and assembly. *Nature* **5:** 908- 919.

Schweiger, A. 2001. Pulsed electron spin resonance spectroscopy: basic principles, techniques, and examples of applications. *Angew. Chem. Int. Ed. Engl.* **30:** 265-292.

Sigurdsson, S.T. and Eckstein, F. 1996. Site specific labeling of sugar residues in oligoribonucleotides: reactions of aliphatic isocyanates with 2' amino groups. *Nucleic Acids Res.* **24:** 3129-3133.

Sigurdsson, S.T., Seeger, B., Kutzke, U. and Eckstein, F. 1996. A mild and simple method for the preparation of isocyanates from aliphatic amines using trichloromethyl chloroformate. Synthesis of an isocyanate containing an activated dissulfide. *J. Org. Chem.* **24:** 3129-3133.

Smith, I.C.P. and Yamane, T. 1967. Spin-labeled nucleic acids. *Proc. Natl. Acad. Sci.* **58:** 884-887.

Stone,T.J., Buckman, T., Nordio, P.L., and McConnell, H.M. 1965. Spin-labeled biomolecules. *Proc. Natl. Acad. Sci.* **54:** 1010-1017.

Tanner, N. K. 1999. Ribozymes: the characteristics and properties of catalytic RNAs. *FEMS Microbiol. Rev.* **23:** 257-275.

Tinoco, I. Jr. and Bustamante, C. J. 1999. How RNA folds. *Mol. Biol.* **293:** 271-281.

Tullius, T.D. and Greenbaum, J.A. 2005. Mapping nucleic acid structure by hydroxyl radical cleavage. *Curr. Opin. Chem. Biol.* **9:** 127-134.

Unrau, P.J.and Bartel, D.P. 1998. RNA-catalysed nucleotide synthesis. *Nature* **395:** 260-263.

Walker, G.C., Uhlenbeck, O.C., Bedows, E., and Gumport, R.I. 1975. T4-Induced RNA ligase joins single-stranded oligonucleotides. *Proc. Natl. Acad. Sci.* **72:** 122-126.

Walter, N.G. 2001. Structural dynamics of catalytic RNA highlighted by fluorescence resonance energy transfer. *Methods* **25:** 19-30.

Wang, Y. H., Murphy, F. L., Cech, T. R., and Griffith, J. D. 1994. Visualization of a tertiary structural domain of the *Tetrahymena* group-I intron by electronmicroscopy. *Journal of Molecular Biology* **236:** 64-71.

Watson, J.D., Baker, T.A., Bell, S.P., Gann, A., Levine, M., Losick, R. 2004. *Molecular Biology of the Gene*, CSHL Press, San Francisco.

Wiegand, T.W., Janssen, R.C., Eaton, B.E. 1997. Selection of RNA amide synthases. *Chem. Biol.***4:** 675-683.

Wilson, T.J., Lilley, D.M. 2002. Metal ion binding and the folding of the hairpin ribozyme. *RNA* **8:** 587-600.

Woodson, S. A. 2002. Folding mechanisms of group I ribozymes: role of stability and contact order. *Biochem Soc Trans* **30:** 1166-1169.

Wu, M., and Tinoco, I., Jr. 1998. RNA folding causes secondary structure rearrangement. *Proc. Natl. Acad. Sci.* **95:** 11555-11560.

VITA

Carré Alison Zalma grew up in Pinckney, MI where she attended numerous schools and participated in a variety of sports. Carré graduated from Stockbridge High School in May 1998. She went on to attend Eastern Michigan University located in Ypsilanti, Michigan where she received her Bachelor of Science degree in the A.C.S. Professional Chemistry program in June 2002. As an undergraduate Carré showed a great interest in research while working under the direction of Dr. Heather L.S. Holmes, Dr. Maria C. Milletti and Dr. Ruth Ann Armitage. These positive female professionals inspired Carré to attend graduate school and continue her constant quest for "understanding how things work". In the fall of 2002 Carré began graduate studies at Texas A&M University. During the following fall she began her thesis work under the direction of Dr. Victoria J. DeRose. She received a Master of Science degree from the Department of Chemistry in December 2005. The author may be reached through her thesis committee member, Dr. David H. Russell; TAMU MS- 3255, Department of Chemistry, College Station, TX 77840.